

Superconductivity and unconventional density waves in vanadium-based kagome materials AV_3Sb_5

Hui Chen(陈辉), Bin Hu(胡彬), Yuhan Ye(耶郁晗), Haitao Yang(杨海涛), and Hong-Jun Gao(高鸿钧)
Citation: Chin. Phys. B, 2022, 31 (**9**): 097405. DOI: 10.1088/1674-1056/ac7f95
Journal homepage: http://cpb.iphy.ac.cn; http://iopscience.iop.org/cpb

What follows is a list of articles you may be interested in

Superconductivity and unconventional density waves in vanadium-based kagome materials AV_3Sb_5

Hui Chen(陈辉), Bin Hu(胡彬), Yuhan Ye(耶郁晗), Haitao Yang(杨海涛), and Hong-Jun Gao(高鸿钧)
Chin. Phys. B, 2022, 31 (**9**): 097405. DOI: 10.1088/1674-1056/ac7f95

Conservation of the particle-hole symmetry in the pseudogap state in optimally-doped $Bi_2Sr_2CuO_{6+\delta}$ superconductor

Hongtao Yan(闫宏涛), Qiang Gao(高强), Chunyao Song(宋春尧), Chaohui Yin(殷超辉), Yiwen Chen(陈逸雯), Fengfeng Zhang(张丰丰), Feng Yang(杨峰), Shenjin Zhang(张申金), Qinjun Peng(彭钦军), Guodong Liu(刘国东), Lin Zhao(赵林), Zuyan Xu(许祖彦), and X. J. Zhou(周兴江)
Chin. Phys. B, 2022, 31 (**8**): 087401. DOI: 10.1088/1674-1056/ac7214

Photothermal-chemical synthesis of P-S-H ternary hydride at high pressures

Tingting Ye(叶婷婷), Hong Zeng(曾鸿), Peng Cheng(程鹏), Deyuan Yao(姚德元), Xiaomei Pan(潘孝美), Xiao Zhang(张晓), and Junfeng Ding(丁俊峰)
Chin. Phys. B, 2022, 31 (**6**): 067402. DOI: 10.1088/1674-1056/ac5604

Experimental observation of pseudogap in a modulation-doped Mott insulator: Sn/Si(111)-(√30×√30)*R*30°

Yan-Ling Xiong(熊艳翎), Jia-Qi Guan(关佳其), Rui-Feng Wang(汪瑞峰), Can-Li Song(宋灿立), Xu-Cun Ma(马旭村), and Qi-Kun Xue(薛其坤)
Chin. Phys. B, 2022, 31 (**6**): 067401. DOI: 10.1088/1674-1056/ac65f2

Evolution of superconductivity and charge order in pressurized RbV_3Sb_5

Feng Du(杜锋), Shuaishuai Luo(罗帅帅), Rui Li(李蕊), Brenden R. Ortiz, Ye Chen(陈晔), Stephen D. Wilson, Yu Song(宋宇), and Huiqiu Yuan(袁辉球)
Chin. Phys. B, 2022, 31 (**1**): 017404. DOI: 10.1088/1674-1056/ac4232

TOPICAL REVIEW — Celebrating 30 Years of *Chinese Physics B*

Superconductivity and unconventional density waves in vanadium-based kagome materials AV_3Sb_5

Hui Chen(陈辉)[1,2,3], Bin Hu(胡彬)[1], Yuhan Ye(耶郁晗)[1], Haitao Yang(杨海涛)[1,2,3], and Hong-Jun Gao(高鸿钧)[1,2,3,†]

[1] *Institute of Physics and University of Chinese Academy of Sciences, Chinese Academy of Sciences, Beijing* 100190, *China*
[2] *CAS Center for Excellence in Topological Quantum Computation, Beijing* 100190, *China*
[3] *Songshan Lake Materials Laboratory, Dongguan* 523808, *China*

(Received 15 April 2022; revised manuscript received 25 June 2022; accepted manuscript online 8 July 2022)

Recently, the discovery of vanadium-based kagome metal AV_3Sb_5 (A = K, Rb, Cs) has attracted great interest in the field of superconductivity due to the coexistence of superconductivity, non-trivial surface state and multiple density waves. In this topical review, we present recent works of superconductivity and unconventional density waves in vanadium-based kagome materials AV_3Sb_5. We start with the unconventional charge density waves, which are thought to correlate to the time-reversal symmetry-breaking orders and the unconventional anomalous Hall effects in AV_3Sb_5. Then we discuss the superconductivity and the topological band structure. Next, we review the competition between the superconductivity and charge density waves under different conditions of pressure, chemical doping, thickness, and strains. Finally, the experimental evidence of pseudogap pair density wave is discussed.

Keywords: kagome metal, superconductivity, charge density wave, pair density wave

PACS: 74.25.−q, 81.05.Zx, 68.37.Ef, 71.45.Lr **DOI:** 10.1088/1674-1056/ac7f95

1. Introduction

Kagome lattice,[1] which is recognized as a sister to the more common hexagonal tiling of graphene, stands out as a model system for the genesis of unconventional electronic and magnetic properties.[2] The kagome lattice can be roughly categorized into the insulating and (semi-)metallic materials. The latter one, especially the transition-metal kagome materials, are of increasing interest due to their potential to manifest non-trivial topologies and unique electronic structures. In most transition-metal kagome lattice materials, the transition-metal elements occupy the vertices of the two-dimensional networks of corner-sharing triangles [Fig. 1(a)]. In contrast to the strongly correlated insulating kagome compounds such as the Herbertsmithite for quantum spin liquids and doped Mott insulators where the geometrical frustration of antiferromagnetic order plays a dominant role,[2–6] these transition-metal compounds are usually correlated metals with itinerant electrons. From the perspective of band theory, the transition-metal kagome materials possess Dirac points and nearly flat bands that naturally promote topological and correlation effects, providing exciting opportunities for exploring frustrated, correlated, and topological quantum states of matter. Remarkable correlated topological phenomena, including massive spin-polarized Dirac fermions,[7–9] magnetic Weyl semimetal,[10–12] topological Chern magnet,[13] negative flat band orbital magnetism,[14] large anomalous Hall effect[15] and spin–orbit polarons,[16] have been observed in the class of Fe-, Co-, and Mn-based magnetic transition-metal kagome shandites [Fig. 1(a)].

Recently, a new family of vanadium-based kagome metals AV_3Sb_5 (A = K, Rb, and Cs) has been discovered by Wilson's group.[17] AV_3Sb_5 unit cell belongs to the space group of $P6/mmm$ (No. 191) and is consisted of a sandwich stacking layer A–Sb2–VSb1–Sb2–A, where alkali metal A forms the hexagonal lattice, Sb2 atoms constitute a honeycomb lattice and Sb1 atoms construct a hexagonal lattice with each Sb1 atom surrounded by six V atoms which are laying on the kagome lattice [Fig. 1(a)]. Due to the unique kagome geometry, the AV_3Sb_5 was predicted to host Z_2 nontrivial topological band structures by calculations based on the density functional theory (DFT).[18] Figure 1(b) shows the typical magnetization and heat capacity characterizations of a CsV_3Sb_5 single crystal.[18,19] The magnetization and specific heat capacity measurement suggest that all materials in the AV_3Sb_5 family exhibit a phase transition at 80–110 K, which corresponds to the charge density wave (CDW) transition. Another phase transition at a lower temperature of 0.9–3 K implies the superconducting (SC) condensation.[18–20]

It is more intriguing that these materials are non-magnetic but exhibit giant anomalous Hall effect (AHE) at low temperature.[21] Unconventional charge orders that break the time-reversal symmetry[22–24] and proximity-induced spin-triplet pairing pointing to an unconventional superconductivity[25,26] have been recently reported. Aside from the evidence for gap nodes and non-trivial core states in magnetic-field induced vortices, the nature of the SC ground state with strong coupling and its correlation to the CDW states have also been reported.[27–29] Moreover, the pair density wave (PDW) was demonstrated with a roton-like behavior and served as a "mother state" corresponding to the pseudogap.[19]

†Corresponding author. E-mail: hjgao@iphy.ac.cn

© 2022 Chinese Physical Society and IOP Publishing Ltd

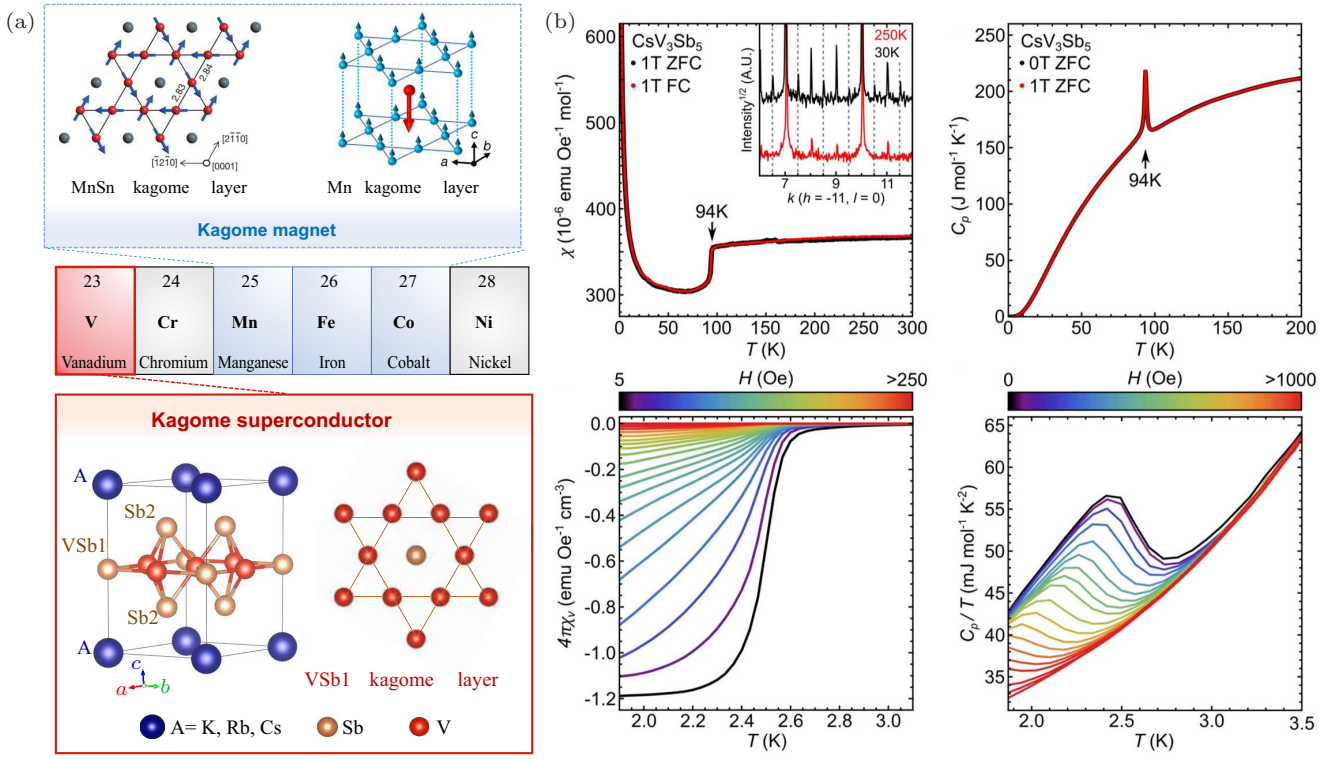


Fig. 1. Discovery of superconductivity and charge density waves in kagome metal AV_3Sb_5. (a) Some elements of transition metals in the periodic table. The Mn-, Fe- and Co-based kagome metals normally host magnetic ground states (the magnetic orders in exemplary MnSn kagome layer in Mn_3Sn[15] and Mn kagome layer in $TbMn_6Sn_6$ [13] are shown in the upper panel), while the V-based kagome metals are found to host superconducting ground states, featuring a kagome superconductor. The atomic models of AV_3Sb_5 and VSb1 kagome layer are shown in the bottom panel. (b) The magnetization and heat capacity measurements of CsV_3Sb_5, showing that the critical temperature of CDW is about 94 K and the critical temperature of superconductivity is about 2–3 K. Adapt with permission from Ref. [18].

In this review, we will focus on the recent studies on the unconventional density waves and superconductivity of AV_3Sb_5. Firstly, we introduce the observations of the AHE, which establish the exploration for the hidden time-reversal symmetry-breaking states. Subsequently, we review the studies of CDWs in AV_3Sb_5 including the $2 \times 2 \times 2(4)$ charge orders in the bulk and unidirectional stripe charge orders observed at Sb surface. The anomalous features including absence of phonon anomaly, rotation symmetry breaking and time reversal symmetry breaking are discussed. Next, we briefly summarize the studies of superconductivity and topological band structures. The competition between superconductivity and CDWs by changing the pressure, chemical doping, thickness, and strain is also presented. Finally, we illustrate the spectroscopic evidence of pair density wave (PDW) state with non-trivial features, promoting further understanding of the similar phenomenon in the cuprates and other superconductors.

2. Emergent giant anomalous Hall effect in AV_3Sb_5

AHE[30–33] is one of the hot topics in the field of condensed matter physics due to its fundamental research interest and exciting applicational prospects. In principle, AHE can be categorized into intrinsic AHE which is mainly induced by the Berry curvature, and extrinsic AHE which is governed by the electrons scattering in the periodic potential of a crystal. The magnetic kagome materials[32–34] due to their bulk gap accompanying the dissipationless edge state, which can contribute to the Berry curvature, are triggering enough research interests in the seeking of AHE, and the typical examples are $Co_3Sn_2S_2$,[32] CoMnGa,[35] and $GdMn_6Sn_6$.[33] More interestingly, the AV_3Sb_5 has been proven to also possess giant AHE[21,36,37] but without magnetic moment.[38]

When performing Hall measurement below the CDW transition temperature, anomalous Hall conductivity can be detected[21,36] [Figs. 2(a) and 2(b)]. Figure 2(c) collects the anomalous Hall properties of more than ten kinds of materials and is divided into three regions depending on the value of longitudinal conductivity σ_{xx}. There are some intriguing features in these results. Firstly, both KV_3Sb_5 and CsV_3Sb_5 show quadratic behavior of σ_{AHE} versus σ_{xx}, and the maximal anomalous Hall conductivity can reach as high as $\sim$ 15507 $\Omega^{-1}\cdot cm^{-1}$ for KV_3Sb_5,[36] and $\sim$ 21000 $\Omega^{-1}\cdot cm^{-1}$ for CsV_3Sb_5,[21] which exceed most of the materials discovered before, showing the discovery of giant AHE without ferromagnetic ordering for the first time in the AV_3Sb_5 family. Secondly, both KV_3Sb_5 and CsV_3Sb_5 are located in similar positions, demonstrating the possible same origin of AHE in the AV_3Sb_5 family. Finally, the experimental anomalous conductivity is much higher than the theoretical calculation value[39] when mainly considering the intrinsic Berry curvature effect,

indicating that the dominant role to control the AHE is the skew scattering. However, Yu *et al.*[21] pointed out that the paramagnetic impurities are about 0.7%. It is still unclear how such low amount of impurities induce the giant anomalous Hall conductivity. On the other hand, Kenney *et al.*[38] claimed that there are no local moments in KV_3Sb_5, directly challenging the skew scattering scenario. In addition, the AHE was found to concurrent with CDW,[21,36,37] which indicates that the mechanism of the AHE is beyond the proposed skew scattering. The discovery of giant anomalous Hall effect starts the exploration for the time-reversal symmetry-breaking states in AV_3Sb_5.

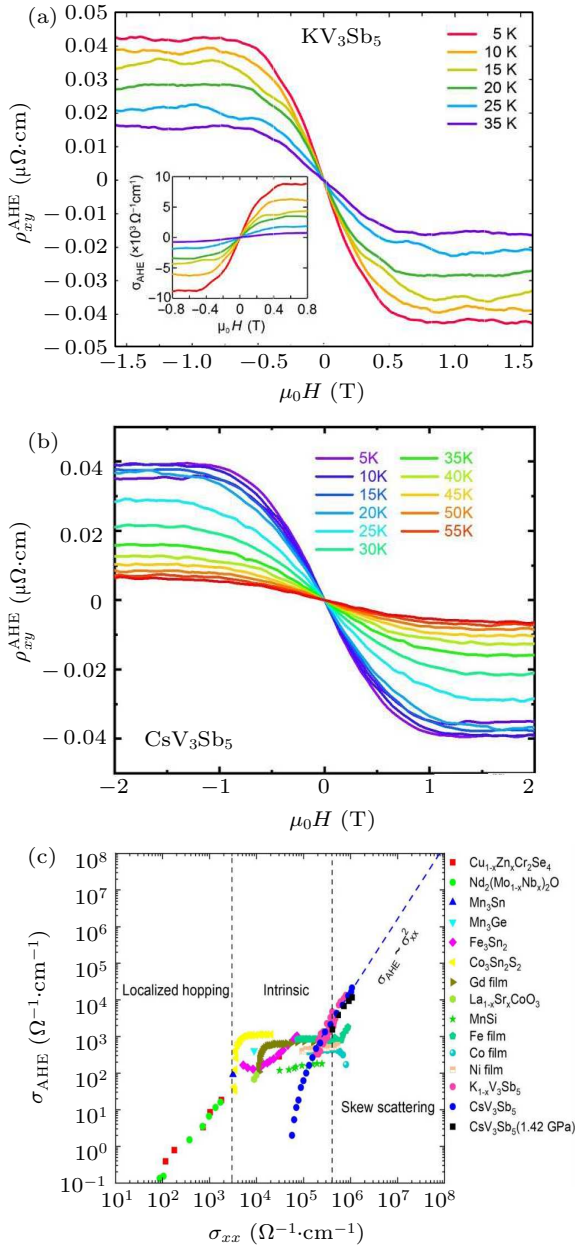


Fig. 2. Giant anomalous Hall effect observed in AV_3Sb_5. (a) AHE in KV_3Sb_5 (adapted from Ref. [36]). (b) AHE in CsV_3Sb_5 at various temperatures (adapted from Ref. [21]). (c) σ_{AHE} versus σ_{XX} for a variety of materials comparing with CsV_3Sb_5 spanning various regimes from localized hopping regime to the skew scattering regime. For CsV_3Sb_5, σ_{AHE} follows quadratic scaling only at low temperature and locates at the same position with $K_{1-x}V_3Sb_5$ (adapted from Ref. [21]).

3. Unconventional charge density wave in AV_3Sb_5

The strong correlation between AHE and CDW raises the questions: what is the origin of the charge orders? Is the time reversal symmetry breaking in the charge orders?

In the situation of one dimension, CDW originates from the combination of electron–phonon coupling and Fermi surface nesting, namely, Peierls distortion.[40] When considering the existence of electron–electron correlations, multiple bands, and spin–orbit coupling in the situation of two or three dimensions, the mechanism of CDW becomes more complex.[41–44] The CDWs in AV_3Sb_5 family exhibit multiple intriguing behaviors with unconventional origins.

3.1. The 2×2 superlattice charge orders in kagome lattice

The phase transition at a critical temperature T^* ranging from 78 K to 103 K is attributed to the CDW phase transition in AV_3Sb_5. The formation of 2×2 superlattice charge order in kagome lattice is firstly evidenced by the early x-ray diffraction (XRD) experiments where the faint superlattice peaks appear at half integer positions below the CDW transition across T^*.[18]

To further study the 2×2 superlattice, low-temperature scanning tunneling microscopy (STM) is applied due to the atomically-precise visualization of the electronic order both in real space and reciprocal space. The CDW transition with 2×2 superlattice modulations is observed by using STM at the temperature below T^*. Figure 3 shows the typical STM results of CsV_3Sb_5. As shown in Figs. 3(a) and 3(b), the Fourier transform of STM topography obtained at Sb surface shows six bright intensity points located at half Bragg reciprocal lattice vectors, directly evidencing the existence of 2×2 charge order in the atomic scale. In general, CDW as the spatial charge density modulation is more relevant to the density of state, which is equivalent to differential conductance maps. And the Fourier transforms of the differential conductance (dI/dV) maps [Fig. 3(c)] show that the 2×2 CDW persists from -300 mV to 200 mV, and show the non-dispersive features.[45] Although STM measurement is performed at the Sb layer, the 2×2 CDW is thought to originated from the underlying kagome lattice as the Sb electronic state contributes little to the charge ordering and tunneling process.[46] Moreover, the temperature-dependent dI/dV spectra exhibits a gap of ~ 20 meV enduring to 78 K and gapless concomitant with the disappearance of 2×2 CDW at 106 K, linking to the T^* of 94 K. Following the discovery of 2×2 charge orders in CsV_3Sb_5, 2×2 CDWs are also evidenced by the Fourier transform of STM topography in KV_3Sb_5[39] and RbV_3Sb_5 [Fig. 3(d)].[23]

The observations of 2×2 superlattice at Sb surface immediately raise a question: whether the CDW modulates along the c-axis. Liang *et al.*[47] revealed a three-dimensional (3D) $2 \times 2 \times 2$ charge order by analyzing the phase information of the CDWs across the single-unit-cell surface step between two

neighboring Cs layers. When focusing on the arrangement of Cs atoms, a π-phase shift between 2×2 CDWs appears to distinguish up and down layers [Fig. 3(e)], suggesting a $2\times2\times2$ CDW in three dimensions. Following the STM observations, the existence of $2\times2\times2$ CDW in the bulk has been further confirmed by many other characterizations.[17,48–51] The CDW peak at half integer L in the XRD measurements proves that the CDWs form a 3D $2\times2\times2$ superstructure [Figs. 4(a) and 4(b)].[17,50] It should be worthy to mention that, both the $2\times2\times2$ CDW[50] and the $2\times2\times4$ CDW for the bulk material[52] have been observed. Very recently, the coexistence of $2\times2\times2$ and $2\times2\times4$ CDW orders was proposed from angle-resolved photoemission spectroscopy (ARPES) measurements.[53]

Both the electron–electron coupling and electron–phonon coupling play a role in the formation of CDW. The Fermi surface displayed combing with the existence of von Hove singularity near the M point[54–56] can satisfy the nesting scenario and give strong indication to form a $2\times2\times2(4)$ CDW which breaks the translational symmetry in the lattice [Fig. 4(c)].[18,52,57] The quantum oscillation measurements on CsV_3Sb_5 evidence that the CDW invokes a substantial reconstruction of the Fermi surface pockets associated with the V orbital and kagome lattice framework.[52] The absence of phonon anomaly in the XRD results [Figs. 4(d) and 4(e)] at the temperature below and beyond T^* implies that the CDW is related to the electron–electron correlation and weak electron–phonon coupling.[50] However, ARPES,[58] optical spectroscopy[59] and the neutron scattering[60] measurements demonstrate that the wave-vector-dependent electron–phonon coupling plays an important role in the CDW order. In addition, recent Raman spectroscopy reported the anomalous amplitude modes in the absence of soft phonons, indicating that the CDW exhibits the character of strong electron–phonon coupling.[61] In the phonon spectroscopy, the structural change shows a predominately first-order phase transition. No CDW amplitude mode is identified in the ordered phase.[62] Similarly, the nuclear magnetic resonance spectroscopy (NMR) measurements show a first-order structural phase transition associated with orbital ordering and a typical second order transition behavior in quadrupole splitting below T_{CDW}.[49,63] These results suggest an unusual coupling between the electron and lattice degrees of freedom, which is different from the traditional CDW condensate.

ARPES measurements reveal complex band structures related to the CDWs. Except for the rich nature of the von Hove singularity,[54–56] the CDW induced band renormalization and energy gaps are observed.[64] The CDW gap shows distinctive momentum dependent features [Fig. 4(f)].[57,58,65]

To understand the anomalies in the experimental studies of the 2×2 superlattice charge order in AV_3Sb_5, there are also some theoretical works on its mechanism. For example, Tan *et al.*[46] found that the pristine lattice structure of AV_3Sb_5 [Fig. 5(a)] is not stable due to the softening acoustic phonon modes at the Brillouin zone boundary near M and L points [Fig. 5(d) for CsV_3Sb_5]. When considering an in-plane 2×2 modulation of the star of David [SD, Fig. 5(b)] or the inverse star of David [ISD, Fig. 5(c)], the imaginary phonon frequency near the M point can be extremely reduced [Figs. 5(e) and 5(f)]. And further including a $2\times2\times2$ reconstruction, the L-point soft mode can be removed as well. The $2\times2\times2$ structure is in agreement with the experimental results.[50] Moreover, all three components in the AV_3Sb_5 family show reduced total energy for SD and ISD structures, and the ISD phase hosts even lower energy than the SD phase [Figs. 5(g)–5(i)]. At the same time, the ISD phase agrees better with experimental results in diffraction pattern,[18] STM image,[39] and transient reflectivity results[48] than the SD phase. Recent ARPES measurements indicate the coexistence of SD and ISD patterns in the AV_3Sb_5.[66] Although many scenarios for the origin of CDWs are proposed by various theoretical works,[46,67–69] the formation mechanisms of the charge orders are still unclear.

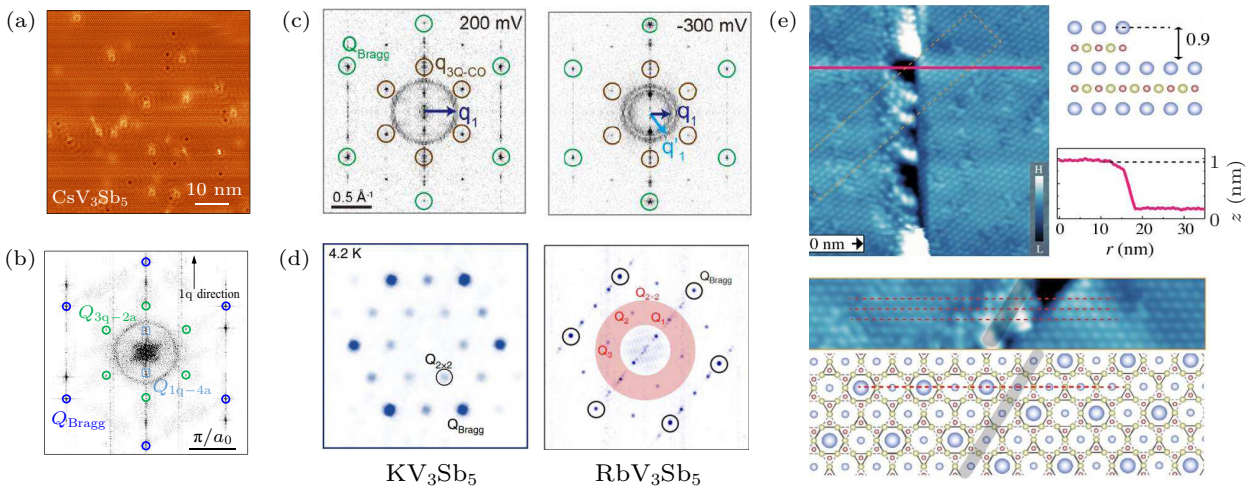


Fig. 3. The 2×2 superlattice charge orders in the kagome lattice of AV_3Sb_5. (a), (b) STM image and corresponding Fourier transform obtained at the Sb surface of CsV_3Sb_5, showing the 2×2 superlattice charge order (adapted from Ref. [19]). (c) Fourier transform of dI/dV map at distinct energy showing the dispersive 2×2 charge order (adapted from Ref. [45]). (d) Observation of 2×2 superlattice at the Sb surface of KV_3Sb_5 (adapted from Ref. [39]) and RbV_3Sb_5 (adapted from Ref. [23]) (e) Illustration of three-dimensional $2\times2\times2$ CDW near a single-unit-cell (adapted from Ref. [47]).

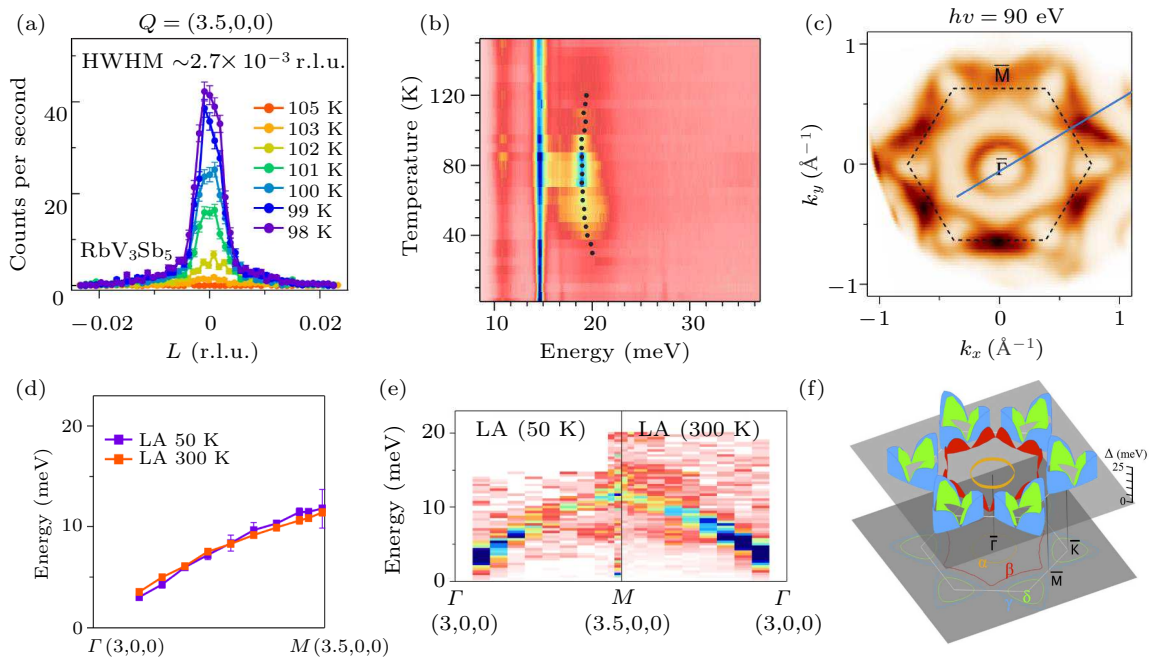


Fig. 4. Unconventional CDW in AV_3Sb_5. (a) Temperature-dependent CDW peaks of RbV_3Sb_5 at $Q = (3.5,0,0)$. (b) Temperature-dependent Raman spectra on CsV_3Sb_5 from 150 K to 3 K. The black dots mark the peak positions of the continuum near 19 meV. (c) Fermi-surface map of RbV_3Sb_5 measured at photon energies of $h\nu = 90$ eV corresponding to $k_z = \pi$ and 0.15π around the $\bar{M}$ point. Data are taken at $T = 15$ K. (d), (e) The IXS determined LA of RbV_3Sb_5 along $\Gamma(3,0,0)$ to $M(3.5,0,0)$ at temperatures of $T = 300$ K and 50 K, where (d) is the extracted-temperature-dependent phonon dispersions from (e) (adapted from Ref. [50]). (f) Three-dimensional plot of the Fermi surface-dependent and momentum-dependent CDW gaps in KV_3Sb_5 (adapted from Ref. [58]).

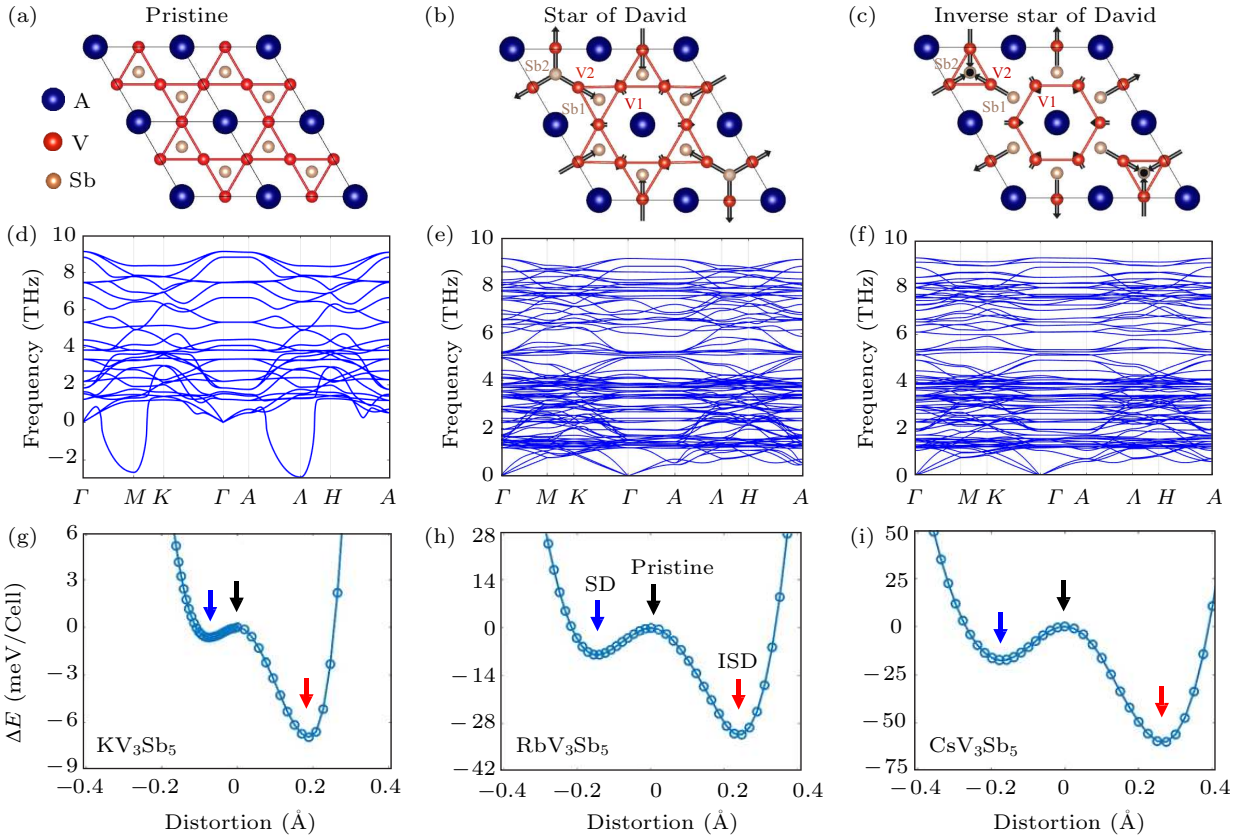


Fig. 5. DFT calculation. Crystal structures of KV_3Sb_5 in the pristine phase, the star of David 2×2 CDW phase, and the inverse star of David phase. Corresponding phonon dispersions are shown in the lower panels. A 2×2 supercell is shown in (a). Imaginary (negative) phonon frequency in (d) corresponds to the breathing mode of the kagome lattice. Such a breathing instability is related to CDW distortions. The breathing out and breathing in lead to two different structures in (b) and (c), where the red arrows indicate the lattice distortion due to the breathing mode. In CDW phases, V1 and V2 represent inequivalent vanadium sites of the kagome lattice, and Sb1 and Sb2 are inequivalent sites of the honeycomb lattice. (g)–(i) Total energy profiles for the three compounds: KV_3Sb_5, RbV_3Sb_5, CsV_3Sb_5, respectively. The distortion stands for the amplitude of the breathing-phonon mode where the negative values are used for star of David (SD) in order to distinguish from inverse star of David (ISD). The ΔE stands for the relative total energy with respect to the pristine phase per supercell (36 atoms). Spin–orbit coupling is considered (adapted from Ref. [46]).

3.2. Rotation symmetry breaking charge orders

In addition to the modulation of c axis for the charge orders, the 2×2 superlattice in the kagome lattice is found to show rotation-symmetry-breaking features. In the Raman measurements, the symmetry is reduced from C_6 to C_2,[48] indicating that three CDW directions are not identical. Li *et al.* found that one of the CDW directions is distinctly different compared with the other two in the Fourier transform of STM topography obtained at the Sb surface of KV_3Sb_5, indicating an intrinsic rotation-symmetry-broken electronic ground state [Fig. 6(a)].[70] Moreover, STM results on the 1×1 Cs surface suggest that the 2×2 CDW breaks the intra-unit-cell rotational symmetry, leading to the electronic nematicity [Fig. 6(b)].[51] This unique two-fold symmetry of the 2×2 CDW arises when temperature below ~ 40 K, indicating the possible introduction of interlayer coupling.[51,71]

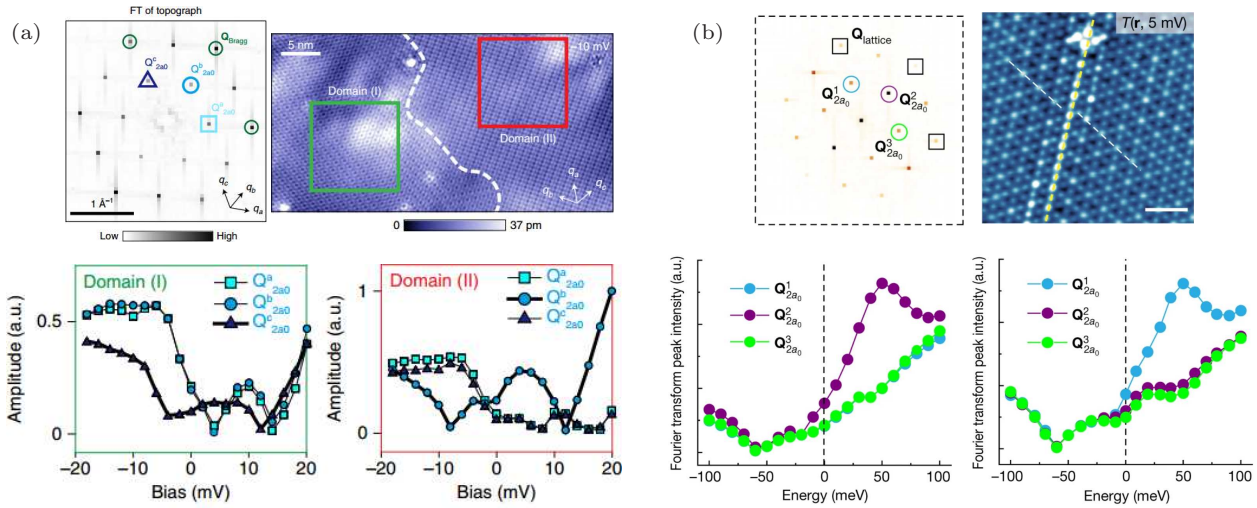


Fig. 6. Rotation symmetry breaking of CDWs. (a) Observation of rotation symmetry breaking 2×2 CDWs at the Sb surface of KV_3Sb_5 (adapted from Ref. [70]). (b) Observation of 2×2 CDWs driven nematicity at the Cs surface of CsV_3Sb_5 (adapted from Ref. [51]).

Besides the rotation symmetry breaking 2×2 CDW in AV_3Sb_5 family, another symmetry breaking order, a featured stripe charge order, is also observed. Although AV_3Sb_5 family share the same crystal structure, the $4a_0$ charge order is mainly observed on the Sb surface of Rb and Cs compounds instead of K compound[19,23,25,39,45] by low-temperature STM, as shown in Figs. 7(a)–7(c). This special charge order can persist to surface defects and step edge[72] [Fig. 7(d)] and occasionally extend to $5a_0$ [Fig. 7(a)]. During the process of imaging in STM, it is found that this $4a_0$ stripe can be shifted with π phase along the scanning direction [Fig. 7(a)], leading to the possibility of CDW engineering.[73,74]

Zhao *et al.*,[45] have systematically investigated the $4a_0$ charge "stripe" modulation and anisotropic quasiparticle interference on the Sb surface of CsV_3Sb_5. There are several significant signals of the $4a_0$ CDW in the Fourier transform [Fig. 7(e)]. Firstly, the $4a_0$ CDW can only exist below the temperature of ~ 60 K, giving its transition temperature. Secondly, its Fourier transform wave vector has a small deviation from the commensurate $4a_0$ period because of the phase slips. Finally, similar to the 2×2 CDW, $4a_0$ peaks are non-dispersive, and thus consistent with the behavior of CDW. In addition, the domain boundary between $4a_0$ CDWs has also been discovered, which further supports the intrinsicality of the rotation symmetry breaking of $4a_0$ CDW, as observed by different STM groups.[19,45]

It is worth noting that the as-obtained large Sb surface usually appears after a special "sweep process" by moving the alkali atoms aside.[19,45] The stripe charge order was only observed on the Sb surface by STM up to now. Different research groups raised the debate whether the $4a_0$ charge order is a surface effect[75] or complex bulk effect.[19,48,76] The origin of the rotation symmetry breaking of the $4a_0$ stripe order as well as the 2×2 CDW needs more experimental evidence and theoretical understanding.

3.3. Time-reversal symmetry-breaking charge order

Since the discovery of the AHE in KV_3Sb_5,[36] muon spin spectroscopy results claim that there is no observable local moment in such material.[38] Subsequently, an STM group from Princeton University[39] inspected the time-reversal symmetry breaking in KV_3Sb_5 by studying the magnetic field response of the 2×2 CDW. Their main results are shown in Fig. 8(a), which consist of three images as the Fourier transforms of STM spectroscopic maps at different magnetic field environments. When the magnetic field is outside the system, the spectroscopic data shows intensity anisotropy at three different directions, and these 2×2 CDW vector peaks are in order clockwise from the lowest to the highest. By introducing a magnetic field, the chirality of 2×2 CDW can be switched from clockwise to anti-clockwise, implying that the 2×2 CDW breaks the time-reversal symmetry. The chiral property of the 2×2 CDW is claimed to exist on the Sb surface of RbV_3Sb_5[23] and CsV_3Sb_5 [75] as well. Most recently, the time-reversal symmetry breaking (TRSB) bounded to the CDW has been evidenced by the muon spin relaxation/rotation experiment as well [Fig. 8(b)].[24]

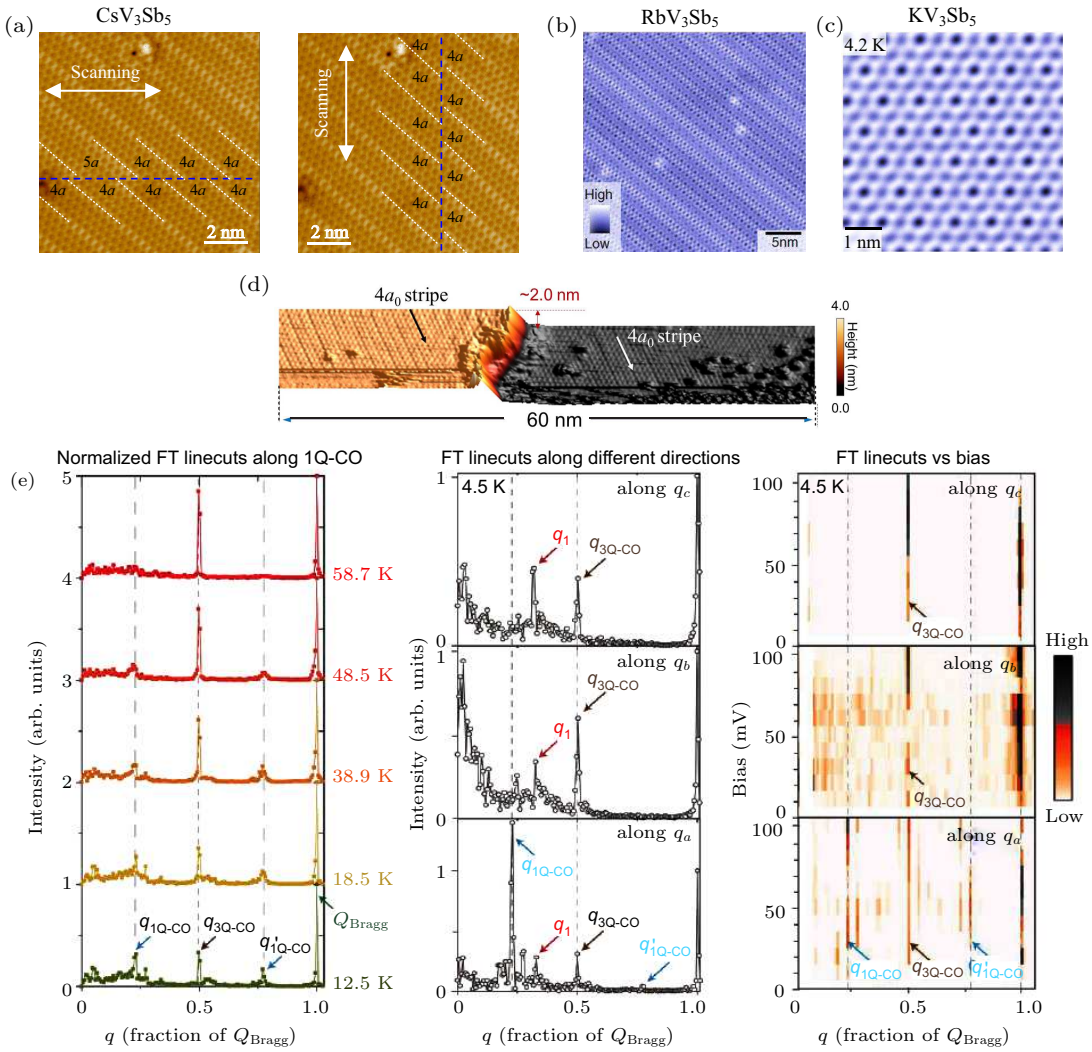


Fig. 7. Stripe charge order in AV_3Sb_5. (a)–(c) STM images of CsV_3Sb_5 (adapted from Ref. [19]), RbV_3Sb_5 (adapted from Ref. [23]), and KV_3Sb_5 (adapted from Ref. [39]), respectively. The positions of the stripes can be spatially shifted along the horizontal direction. Occasionally, the distance between two neighboring stripes changes from $4a_0$ to $5a_0$. (d) Observation of stripe order across the step edge (adapted from Ref. [72]). (e) The Fourier transform signal of stripe order at various temperatures, along different directions and at distinct scanning bias, showing that the non-dispersive and unidirectional stripe order disappears around 60 K (adapted from Ref. [45]).

To further understand the phenomenon of the TRSB of the 2×2 CDW, Feng *et al.*[67] introduced a chiral flux phase (CFP) in the AV_3Sb_5 family. Based on a 2D model, and depending on the order parameter, a vector CDW, a charge bond order, and a charge CFP can be formed. The CFP has the lowest ground state energy compared with the other orders. Its relative charge configuration is shown in Fig. 8(c), in which two types of current flux loops form honeycomb lattice and hexagonal lattice are marked by red circle and blue circle, respectively. Combining these two distinct loops naturally gives rise to a 2×2 charge order. The Chern number is equal to 1 in the CFP by calculating the intrinsic Hall response, which can further support the results in Hall transport measurements, where the non-quantized experimental Hall resistance may result from the complex multi-orbital effect. Furthermore, the same theoretical group[77] found as many as 183 flux phases on a kagome lattice within 2×2 unit cell after the proposed CFP and completed the classificational work by symmetry inspection. And a parallel theoretical work based on mean-field analysis was also proposed by Dinner *et al.*[68]

Yu *et al.*[22] claimed that the as-observed TRSB signal in zero-field muon spin relaxation experiment can be the evidence of chiral flux phase, but the transition temperature resides around 70 K, which does not fit the CDW transition temperature, may correspond to another hidden order. Meanwhile, Jiang *et al.*[39] stressed that the chiral feature of 2×2 CDW can only occur at the surface defect-free region, but another STM group[70] denied the chirality and its filed tunability of CDW by using the low-temperature STM in KV_3Sb_5 samples grown from the same group. Moreover, Li *et al.*[78] claimed that such chiral flux current in CsV_3Sb_5 is not observed by utilizing the spin-polarized STM. Some optical experiments also provided strong evidence for detecting the TRSB. Xu *et al.*[79] performed scanning birefringence microscopy, magneto-optical Kerr effect and circular dichroism measurements and showed that in AV_3Sb_5 system both a three-state nematicity and TRSB exhibit at T_{CDW}. Bulk symmetry breaking state with two-fold rotation symmetry in charge-density-wave was reported by Wu *et al.* using the optical polarization rotation method.[80]

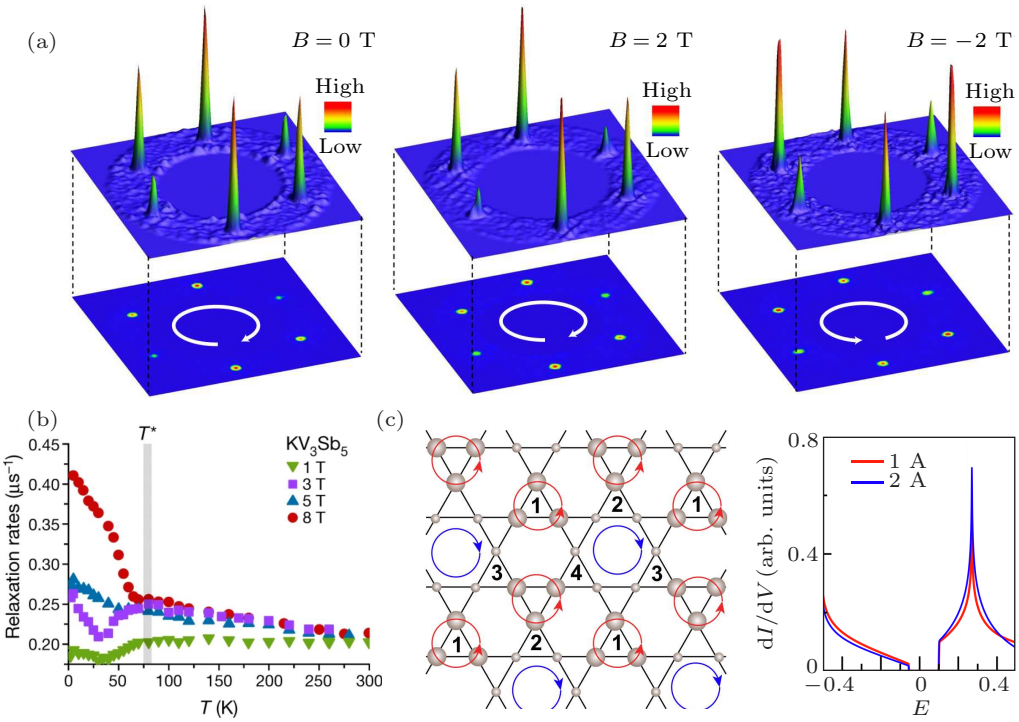


Fig. 8. Time reversal symmetry breaking charge order in AV_3Sb_5. (a) Spectroscopic 2×2 vector peaks taken at the impurity-pinning-free Sb surface region of KV_3Sb_5 by applying the magnetic field $B = 0$ T, $+2$ T and -2 T, respectively, showing that the strength of intrinsic charge modulations exhibits chiral anisotropy with unusual magnetic field response (adapted from Ref. [39]). (b) The temperature dependence of the muon spin relaxation rate, showing the enhanced magnetic response of the charge order with applying external magnetic fields (adapted from Ref. [24]). (c) Theoretical prediction of chiral flux phase in the kagome superconductor AV_3Sb_5 (adapted from Ref. [67]).

The TRSB is alluring in the field of condensed matter physics, and the discovery of the TRSB[39] in AV_3Sb_5 family has aroused enough research interests in the past two years. However, for a deeper understanding of the underlying mechanism, it still needs more experimental evidence, especially for the smoking-gun-like proof, and further theoretical proposal to connecting the diverse experimental results. Except for the theoretic works mentioned here, there are different proposals[68,69,81,82] postulated to try to uncover the underlying physics.

In this section, we have shown various experimental evidence of $2 \times 2 \times 2(4)$ CDW in AV_3Sb_5 at first. Although the Fermi surface nesting and electron–phonon coupling can mainly account for its mechanism, different experimental results favor to support the electron–electron correlation scenario. The $2 \times 2 \times 2(4)$ CDW with momentum-depend energy gap was demonstrated by several ARPES groups, but the physics behind is still an open question. Besides, the rotation symmetry breaking states including the unidirectional $4a_0$ charge order and electronic nematicity stimulate new research interest. Surprisingly, the discovery of TRSB bridges the $2 \times 2 \times 2(4)$ CDW to AHE and promotes the understanding the origin of the AHE.

4. Superconductivity in AV_3Sb_5

In addition to the anomalous charge orders, another intriguing property for AV_3Sb_5 is the superconductivity. The research of superconductivity has triggered enough interests in many materials for a very long time,[83–88] especially for the unconventional superconductivity among the new materials in the past decades, such as cuprates,[89–91] iron-based superconductors,[92–94] and Ni-based superconductors.[95–97] Understanding the mechanism of superconductivity is of great significance in condensed matter physics. The kagome superconductors AV_3Sb_5 provide a new platform to understand and tune the superconductivity. Furthermore, the V-based superconductors may also contribute to the long sought-after topological superconductors,[98–101] which are the footstones for quantum computing.[102,103]

4.1. Basic characterizations of superconductivity

Despite the transport measurements have justified the superconductivity of all three kagome materials in the AV_3Sb_5 family,[18,37,104] the microscopic evidence is still lacking. For the superconductivity, there are several key issues that are worthy to be addressed.

4.1.1. Strong coupling or weak coupling?

For CsV_3Sb_5, the spatially-averaged local densities of state on both Sb and Cs surface show V-shaped feature and finite zero-bias conductance [Fig. 9(a)]. The spectrum on the Sb layer exhibits a deeper zero-energy conductance and a sharper coherence shoulder than on the Cs layer at electron temperature of 300 mK.[19] The transition temperature of the superconductivity deduced from the temperature-dependent experiments is ~ 2.3 K [Fig. 9(b)]. To further elucidate that the as-observed spectra are the superconductor density of state,

a Josephson junction by using a superconducting tip is constructed [Fig. 9(c)]. The significant signals of the Josephson effect are shown in Fig. 9(d). Additional, two thermal-induced symmetric in-gap peaks appear when temperature increases, and disappear at about ~ 2.3 K, which is consistent with the normal tip case.[19] Based on the spatially-averaged superconducting gap size of ~ 0.52 meV over the whole sample surface and transition temperature, the gap-to-T_c ratio $2\Delta/k_BT_c$ is ~ 5.2, indicating a strong-coupled superconductivity from the perspective of local STM measurements.[19] On the other side, in the heat capacity measurements of KV_3Sb_5 [Fig. 9(e)], the fitted dimensionless specific jump at superconducting transition temperature (T_c) is estimated to be $\Delta C_{es}/(\gamma_n T_c) = 1.03$, which is quite small relative to the BCS weak coupling limit ($\Delta C_{es}/(\gamma_n T_c) = 1.43$). The inconsistence between the STM and heat capacity measurements suggests possible anisotropic gap function or multigap for the AV_3Sb_5.

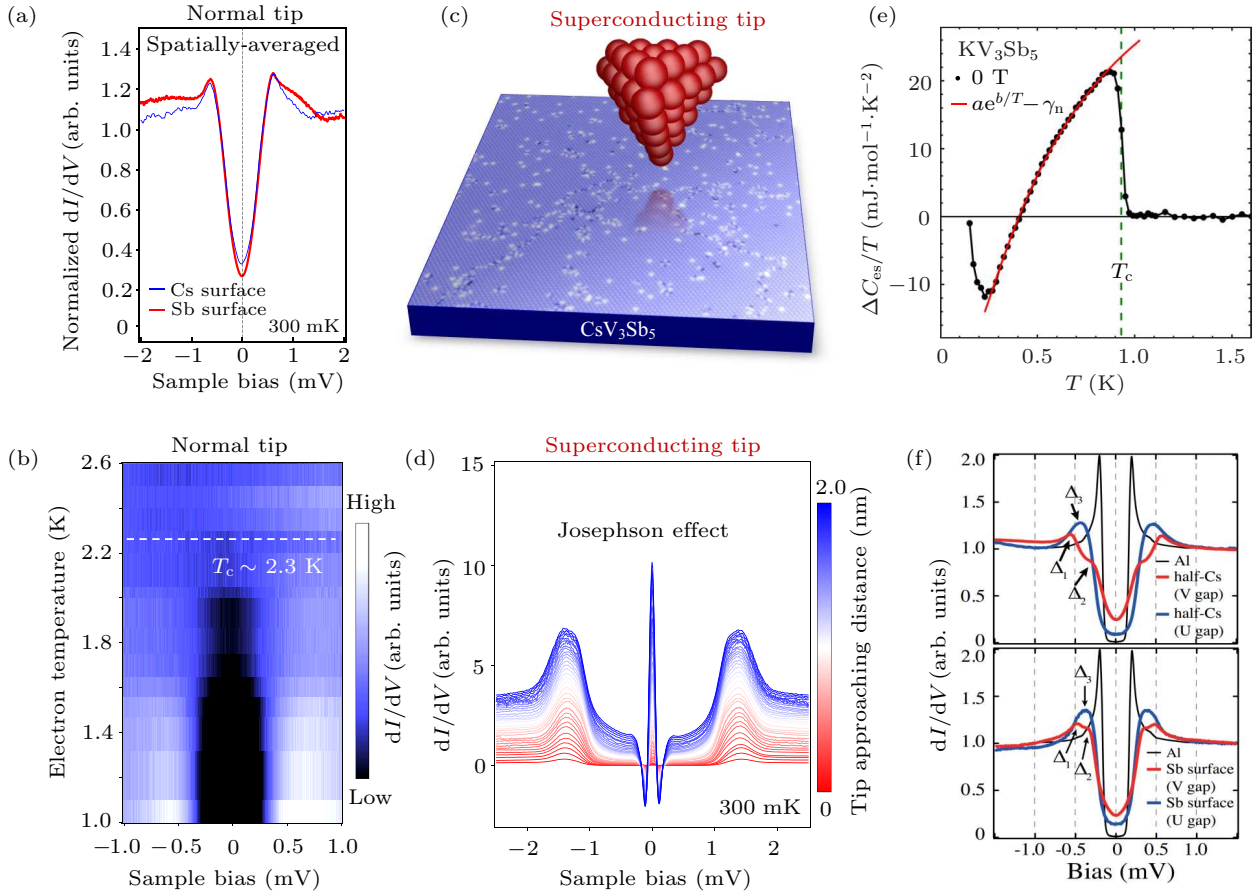


Fig. 9. Observation of superconductivity in AV_3Sb_5. (a) Spatially-averaged dI/dV spectra obtained on the Cs and Sb surfaces of CsV_3Sb_5, showing a particle-hole symmetric V-shaped gap near E_F and non-zero LDOS at zero-bias. (b) Color map of temperature dependent dI/dV spectra showing the disappearance of V-shaped gap at about 2.3 K. (c), (d) The observation of Josephson effect by using a superconducting tip, which provides strong evidence that the CsV_3Sb_5 is in the SC phase (adapted from Ref. [19]). (e) The specific heat capacity difference between the superconducting and normal states of KV_3Sb_5. The fitted dimensionless specific jump at T_c indicates a weak coupling superconductivity (adapted from Ref. [104]). (f) dI/dV spectra with ultra-high energy resolution, showing multiband superconductivity in CsV_3Sb_5 (adapted from Ref. [25]).

4.1.2. Single-gap or multigap?

The SC gap in dI/dV spectra of most low-temperature STS measurements shows a single SC gap near 0.5 meV. But it does not fit the single-gap Dynes function, implying the possible multi-band attribution of the superconducting state.[47] Meanwhile, Xu *el al.* reported two kinds of SC gaps with multiple set of coherent peaks and residual zero-energy density of states at both Cs and Sb surfaces [Fig. 9(f)], indicating that the superconductivity has band-dependent gap functions.[25] In addition, the temperature-depended curves of critical field in the transport measurements fit well with a two-gap model [Fig. 10(a)][105] and the temperature dependence of the in-plane and out-of-plane components of the magnetic penetration depth[106] further support the multi-band nature of the superconductivity.

4.1.3. Isotropic or anisotropic?

Applying a magnetic field to CsV_3Sb_5, the zero-temperature out-of-plane and in-plane upper critical fields are determined to be 0.8 T and 7.2 T, respectively [Fig. 10(a)]. The coherence length for out-of-plane and in-plane can be deduced to be 2.2 nm and 20.3 nm, separately. And the lower critical fields along the two directions are both lower than 5 mT. Meanwhile, Ni *et al.*[105] found that the angular-dependent magnetoresistance (AMR) shows a prominent two-fold symmetry under a magnetic field of 0.5 T in the mixed state, and

the AMR slips 60° when the temperature changes from 2.8 K to 2.6 K. The origin of the observed AMR twist is not yet clear. Similar two-fold symmetry in the superconducting state was reported by Xiang *et al.*[76] [Fig. 10(b)].

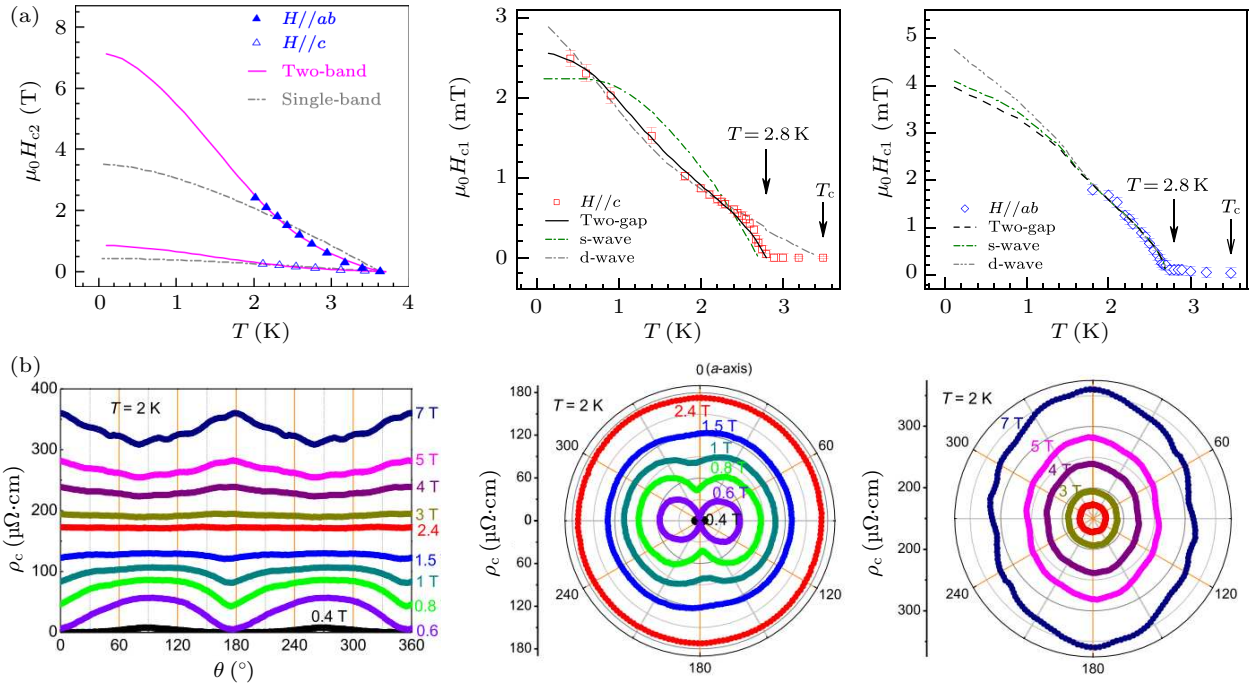


Fig. 10. Anisotropic superconducting properties of CsV_3Sb_5. (a) Temperature dependence of the upper critical fields and the lower critical field, showing that the upper critical field exhibits a large anisotropic ratio at zero temperature and fitting its temperature dependence requires a minimum two-band effective model (adapted from Ref. [105]). (b) The *c*-axis resistivity with the in-plane rotation of magnetic field showing a two-fold symmetry of superconductivity in the superconducting state and a unique in-plane nematic electronic state in normal state when rotating the in-plane magnetic field (adapted from Ref. [76]).

4.1.4. Nodal or nodaless?

The V-shaped feature and finite zero-bias conductance in the dI/dV spectra of CsV_3Sb_5 [Fig. 9(a)] cannot be obtained from the thermal broaden of a gapped superconductor spectrum at low temperature, indicating that the gapless states coexist with the superconductivity at zero temperature.[19] Besides, the muon spin relaxation/rotation measurement suggests that the superconductivity does not break the time-reversal symmetry and shows unconventional nature.[106] In addition, the density-functional theory calculation shows that the electron–phonon coupling is too weak to account for such high superconductor transition temperature, implying the unconventionality of the superconductivity.[46] On the other hand, s-wave full gap superconductivity was uncovered by the $^{121/123}$Sb NQR and ^{51}V NMR measurements.[107] The in-gap states in the dI/dV spectra could be induced by magnetic impurities but not by nonmagnetic impurities, suggesting a sign-preserving or s-wave superconducting order parameter.[25] Based on the geometric structure of the kagome lattice, some theoretical models have been proposed to try to understand the mechanism of superconductivity and the observable low energy behavior,[26,108] a satisfactory model to reconcile all experimental results about AV_3Sb_5 is still lacking.

4.2. Possible topological superconductor candidate

Another interesting property of AV_3Sb_5 kagome materials is the combination of superconducting ground state with intrinsic Z_2 topology, where the protected Dirac crossings are close to the Fermi level. The topological surface states are firstly proposed by the DFT calculations as well. Figure 11(a) shows the calculated band structure of CsV_3Sb_5, and displays the Z_2 topological invariant obtained by checking the parity of the wave function at the time-reversal invariant moment. Focusing on the surface state near the $\bar{M}$ point, there are Dirac crossings at the energy of about 0.05 eV above the Fermi energy, as shown in Fig. 11(b). Such surface states show anisotropic dispersions between $\bar{M}-\bar{\Gamma}$ direction and $\bar{M}-K$ direction [Fig. 11(b)]. The Z_2 topology is proposed for all three materials of AV_3Sb_5 family including the pristine, star of David and inverse star of David structures.[46] The topological surface states are evidenced by the ARPES measurement as shown in Figs. 11(c) and 11(d).

The vortex bound states have been proved to be an ideal platform to study the topological nature of superconductors. The superconducting gap gradually induces with increasing the magnetic field perpendicular to the sample surface. When applying a magnetic field of tens of milli-Tesla perpendicular to the surface, the Abrikosov-vortices lattice is observed both at Cs surface and Sb surface.[19,25,47] However, the dI/dV linecuts crossing the vortex core on the two surfaces show distinct behaviors. The bound states inside the vortex core collected at Sb surface exhibit a X-type evolution with spatial distance, while the ones at Cs surface exhibit Y-type evolution with a broad zero-bias peak at the core center [Figs. 12(a)

and 12(b)]. The X-type in-gap core states are usually thought to be trivial as it has been widely observed in conventional s-wave superconductors.[109–111] On the other hand, the Y-type features of in-gap core states may indicate the presence of Majorana bound states as reported in other superconductors with topological surface states.[112]

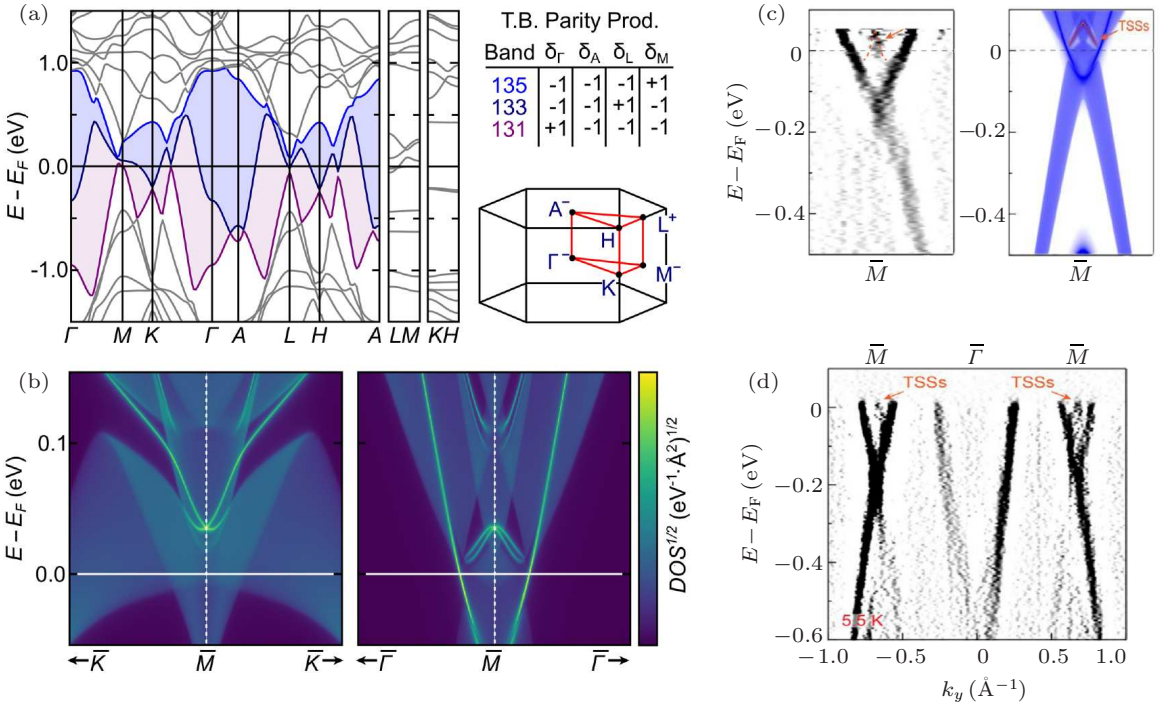


Fig. 11. Topological band structures of CsV_3Sb_5. (a) Calculated band structure of CsV_3Sb_5 along high-symmetry directions across the Brillouin zone. A continuous direct gap (shaded) is noted and high-symmetry points in the Brillouin zone are labeled. (b) Tight-binding model of CsV_3Sb_5 showing topologically protected surface states that manifest at the time-reversal invariant momentum $\bar{M}$ point (adapted from Ref. [18]). (c)–(d) Observation of topological surface state above the CDW transition temperature (c) and at 5 K (d) (adapted from Ref. [114]).

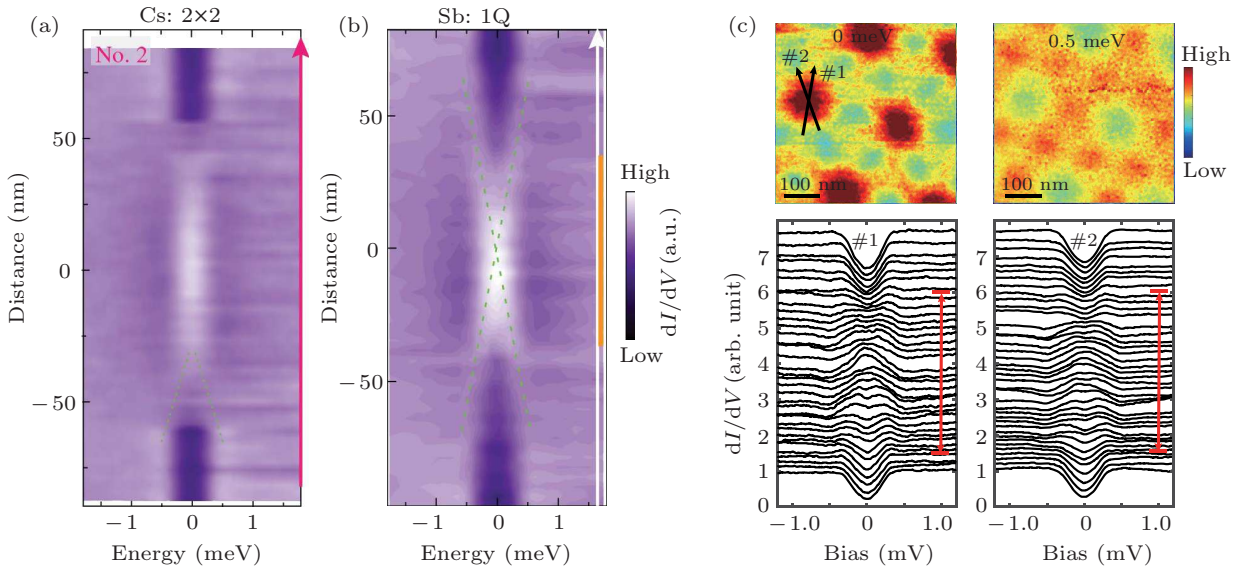


Fig. 12. Vortex core-states in CsV_3Sb_5. (a), (b) Color map of the spatially resolved dI/dV spectra across the vortex at Cs and Sb surfaces, respectively, showing surface-dependent vortex-core states (adapted from Ref. [47]). (c) Vortex states measured on the Sb surface of CsV_3Sb_5 with ultra-high energy resolution, showing Caroli–de Gennes–Matricon states instead of zero-bias vortex bound states in the vortex core (adapted from Ref. [25]).

If the as-observed zero-bias peak is originated from Majorana bound states, how the Dirac surface states become superconducting as the calculated topological surface state is about 0.05 eV above the Fermi surface? One possibility is electronic reconstructions and doping effect induced by the alkali atom desorption.[113] Another possibility is the CDW state induced band shift evidenced by a recent ARPES work,[114] where the observed topological surface states are very close to the Fermi surface and further move down in the CDW state [Fig. 11(c)]. Comparing to the calculation, the lower energy of the topological surface states in the real materials activates the topological states for electron conduction in the superconducting state at

low temperature [Fig. 11(d)]. To prove that AV_3Sb_5 family serve as an eligible candidate for the topological superconductor, ultralow temperature STM measurements and more experimental evidence are needed. It should be noticed that recent STM works with higher energy resolution claim that the broad peak in the near vortex core is asymmetric for the vortices at both Cs and Sb surfaces, which is consistence with Caroli–de Gennes–Matricon states instead of the zero-energy vortex bound states [Fig. 12(c)].[25]

5. Competition between charge density wave and superconductivity

CDW and SC are similar in the perspective of mean field theory. They are both related to the electron–phonon coupling and Fermi surface instability, or affected by electron–electron interactions. In most cases, CDW is competing with SC,[115–117] and the situation in AV_3Sb_5 family is no exception, especially under distinct pressure, chemical doping contents, thickness, and strains.

5.1. High pressure

The AV_3Sb_5 kagome superconductor shows an unusual competition of superconductivity and CDW. By applying pressure on the CsV_3Sb_5, the CDW is suppressing monotonically, which is accompanied by the increase of SC, showing the competition between CDW and SC.[20,118] It is rational to expect such competition since the released density of state from the suppressed CDW state will contribute to the enhancement of SC. By a closer inspection of the pressure-dependent T_c of SC, two-dome feature is observed, where the T_c shows two broad peaks at ~ 0.7 GPa and 2.0 GPa with carrying a dip at ~ 1.1 GPa [Fig. 13(a)].[118] The highest peak corresponding to 2.0 GPa is up to 8 K. Meanwhile, the upper critical magnetic field shows the same behavior as T_c [Fig. 13(a)], and the maximal value is as high as ten times larger than the initial one at ambient pressure.[118] The double superconducting dome is widely discovered in AV_3Sb_5 family,[20,119–122], which manifests the non-trivial SC as well as the unconventional CDW [Fig. 13(b)].[122]

The superconducting phase is also tuned by the high pressure due to the suppress of CDW. If the pressure increases further to 150 GPa, a new superconducting phase appears which is rather robust and inherently lined to the interlayer Sb2–Sb2 interactions [Fig. 13(c)].[123] The formation of Sb2–Sb2 bounds at high pressure tunes the system from two-dimensional to three-dimensional and pushes the p_z orbital of Sb2 upward across the Fermi level, resulting in enhanced density of states and increase of T_c. In a recent pressure-tuned and ultra-low temperature muon spin spectroscopy, the superconducting state displays a nodal energy gap and a reduced superfluid density competing with a time-reversal-symmetry breaking charge order under low pressure. However, under high pressure, the charge-order transitions are suppressed, the superfluid density increases and the superconducting state progressively evolves from nodal to nodeless.[124]

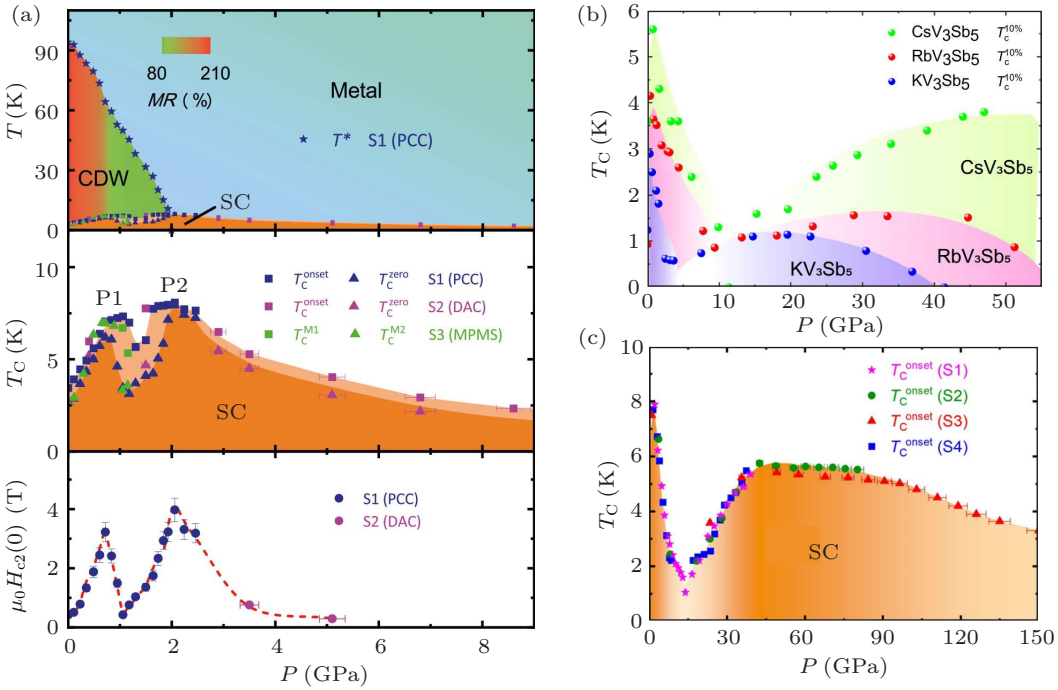


Fig. 13. Phase diagram with pressure for AV_3Sb_5. (a) Phase diagram of CsV_3Sb_5 with pressure, showing the unusual competition of superconductivity and charge-density-wave (adapted from Ref. [118]). (b) Temperature-pressure phase diagram of AV_3Sb_5 (A = Cs, Rb and K), showing the universal double-dome superconductivity under pressure (adapted from Ref. [122]). (c) The high-pressure electrical measurements up to 150 GPa, showing a new superconducting phase to be rather robust (adapted from Ref. [123]).

5.2. Chemical doping

Another approach to study the competition between SC and CDW is the chemical doping. To avoid killing the superconductivity, doping elements should be carefully selected since AV_3Sb_5 with much deficiency will not produce superconductivity.[17,18] The earliest attempt to bring superconductivity into the potassium-deficient and non-superconductive $K_{1-x}V_3Sb_5$ was done by Wang *et al.*,[125] where they successfully fabricated a Josephson junction with $K_{1-x}V_3Sb_5$, and introduced the spin-triplet Cooper pairs by the proximity effect. So far, two types of chemical doping through substation of partial elements have been achieved in experiments. One type is the chemical doping into the non-superconducting layer such as substation of Sn onto the Sb layer. The phase diagram for $CsV_3Sb_{5-x}Sn_x$ shows a doping effect where the nearest van Hove singularity is shifted toward and above E_F. The superconductivity exhibits a non-monotonic evolution with doping content, resulting in two "domes" peaked at 3.6 K and 4.1 K and the rapid suppression of CDW [Fig. 14(a)].[126] The other type is the direct substitution of other 3d transition metal elements onto the V site in the kagome superconducting layer. The phase diagram for the $CsV_{3-x}Ti_xSb_5$ shows a doping effect as well. Ti doping induced two distinct phases have been discovered. The slightly-doped SC phase has a V-shaped SC gap, coexisting with CDW and AHE, indicating a strong-coupling unconventional SC nature. The highly-doped SC phase has a U-shaped SC gap where the CDW and AHE are undetectable.[127] The T_c in the Ti-doped sample has a little enhancement to about 3.5 K. For the Nb-doped system, the T_c is enhanced monotonically to about 4.45 K.[128]

5.3. Thickness

The competition between CDW and SC is also observed in sample-thickness-depend experiments.[27] The evolution of CDW and SC with sample thickness in CsV_3Sb_5 shows that the T^* decreases from 94 K in bulk to a minimum of 82 K at thickness of 60 nm, then increases to 120 K as the thickness is further reduced to 4.8 nm. The T_c shows an exactly opposite evolution, increasing from 3.64 K in the bulk to a maximum of 4.28 K at thickness of 60 nm, then decreasing to 0.76 K at 4.8 nm.[27] Song *et al.* also observed the competition of SC and CDW in selective oxidized CsV_3Sb_5 thin flakes. The prominent effect of hole doping is achieved by the selective oxidation, which induces a superconducting dome as a function of the effective doping content. The T_c and upper critical field in thin flakes are significantly enhanced compared with the bulk ones[28] [Fig. 14(b)].

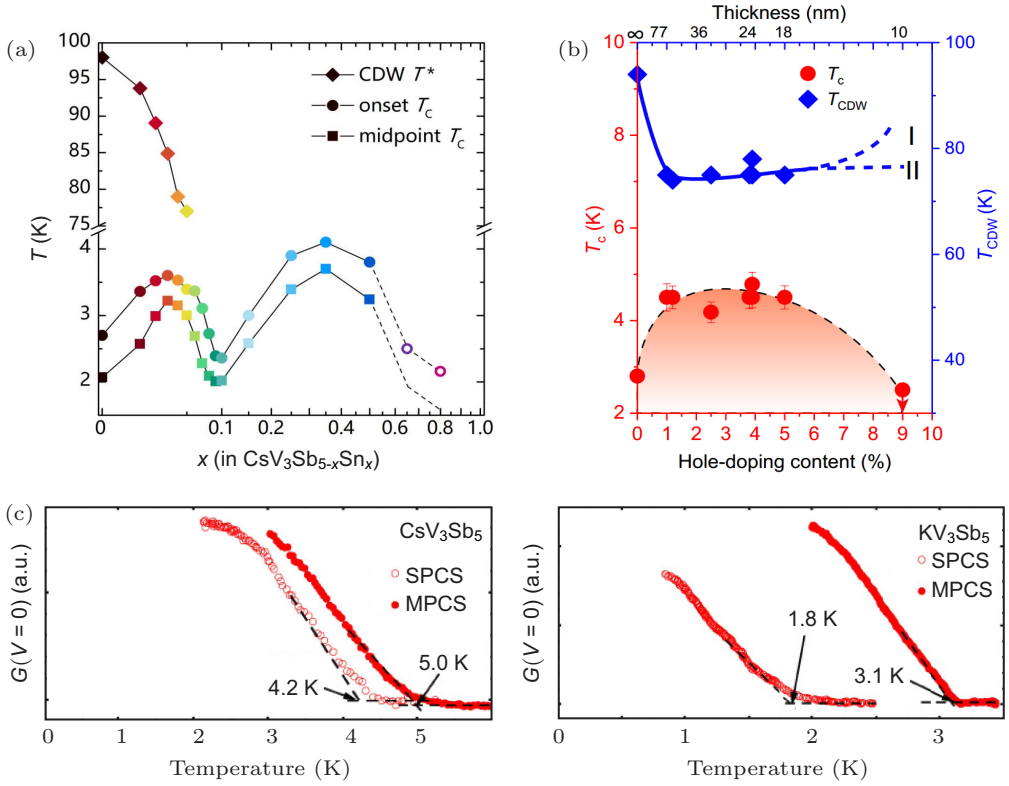


Fig. 14. Phase diagram with chemical doping, thickness, and strain for AV_3Sb_5 crystal. (a) Hole-doping phase diagram for $CsV_3Sb_{5-x}Sn_x$, showing the suppression of CDW and double-dome superconductivity with increasing doping contents (adapted from Ref. [126]). (b) Phase diagram of CsV_3Sb_5 with the variation of hole-doping content, where only the top layer is assumed to be oxidized, showing the competition of superconductivity and charge density wave in selective oxidized CsV_3Sb_5 thin flakes (adapted from Ref. [28]). (c) Point-contact spectroscopy at CsV_3Sb_5 and KV_3Sb_5, showing strain-sensitive superconductivity (adapted from Ref. [129]).

5.4. Strain

The stain-sensitive SC in KV_3Sb_5 and CsV_3Sb_5 has been observed in point-contact spectroscopy. T_c is enhanced in soft point contact spectroscopy and further enhanced in mechanical point-contact spectroscopy. The enhanced SC probably arises from local strain caused by the point contact, which leads to two-gap or single-gap behaviors observed in different point contacts[129] [Fig. 14(c)].

The competition between the CDW and SC provides the key clue for us to further increasing the T_c of SC while suppressing the CDW. When the T_c of SC goes beyond the helium-4 temperature range, the possible application may come out for the first generation. Meanwhile, AHE could be realized at a higher temperature if reducing the SC, since the CDW is intimately related to the AHE. Besides, the competition between CDW and SC provides a new platform for investigating the behavior of electrons in such a fertile system.

6. Pair density wave in CsV_3Sb_5

When Cooper-pairs spatially modulate with a wave vector Q, the Cooper-pair density wave can occur. Historically, PDW was confirmed in only a few systems[130–133] due to the limitation of ultra-high spatial resolution technique and candidate of materials. Thanks to the ability of atomically-precise visualizing the density of state in both real and momentum spaces, spectroscopy-image STM becomes the a powerful tool in the progress of searching PDW.

Recently, a pseudogap PDW was found in CsV_3Sb_5 by the utilization of STM. Except for the 2×2 CDW and $4a$ CDW in Fourier transform of topography [Figs. 15(a) and 15(b)], three pairs of new peaks with significant intensity at wave vectors $\boldsymbol{Q}_{3q-4-a/3}=\frac{3}{4}\boldsymbol{Q}^{(a,b)}_{\rm Bragg}$ appear in the Fourier transform [Fig. 15(d)] of $\mathrm{d}I/\mathrm{d}V$ map at the energy of -5 meV [Fig. 15(c)]. These newly appeared peaks indicate a new electronic order. These peaks are observed at the energy between $+5$ meV and -5 mV and nondispersive [Fig. 15(e)], suggesting a hidden $3Q$ density wave relates to the superconducting state. By filtering the noisy around the origin and atomic Bragg peaks at $Q_{\rm Bragg}$ in the Fourier transform image, the spatial modulation of the $3Q$ density wave [Fig. 15(f)] is clearly visible.

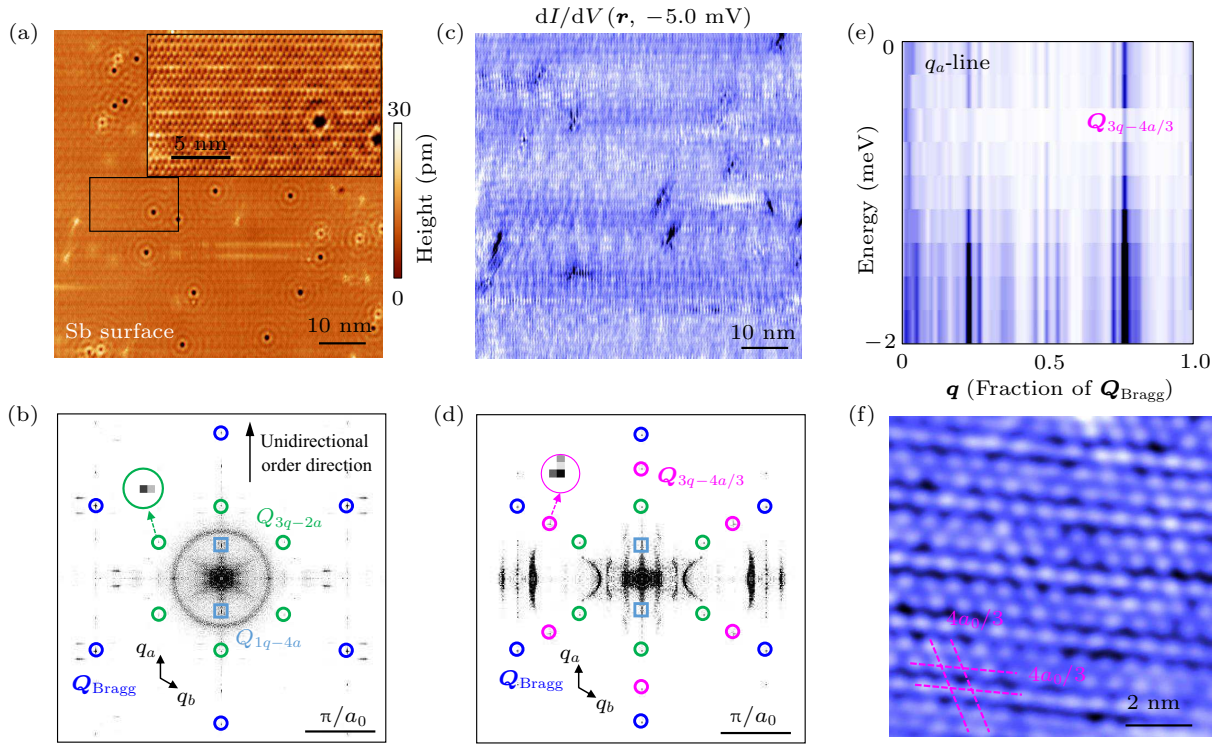


Fig. 15. Observation of a new density wave at $Q_{3q-4a/3}$ in CsV_3Sb_5. (a)–(d) The large-scale STM topography, $\mathrm{d}I/\mathrm{d}V(\boldsymbol{r},-5\,\mathrm{mV})$ map of Sb surface and corresponding Fourier transforms, showing the discovery of a new superlattice at $Q_{3q-4a/3}$ highlighted by the magenta circles beyond 2×2 and 1×4 orders. (e) Energy dependence of the Fourier line cuts along one lattice direction as a function of energy, respectively, showing non-dispersive ordering vectors at $Q_{3q-4a/3}$. (f) $\mathrm{d}I/\mathrm{d}V(\boldsymbol{r},V)$ map near the pairing gap at 0.4 mV, after filtering out atomic Bragg peaks and incoherent background, exhibiting $4a/3$ checkerboard modulation associated with the bidirectional PDW (adapted from Ref. [19]).

The observations of SC gap modulating at the same wave vectors demonstrate that the $3Q$ density wave is a PDW. In the one-dimensional case, the $\mathrm{d}I/\mathrm{d}V$ linecut along the $4a$ stripe direction demonstrates that the SC gap $\Delta(\boldsymbol{r})$, zero-energy conductance ($G_0(\boldsymbol{r})=\mathrm{d}I/\mathrm{d}V(\boldsymbol{r},0)$), and coherence peak height ($P(\boldsymbol{r})=\mathrm{d}I/\mathrm{d}V(\boldsymbol{r},+\Delta(\boldsymbol{r}))$) spatially modulate in a period of $4a/3$ [Figs. 16(a)–16(d)]. To see the spatial modulation of the SC gap clearly, the second derivative is applied to the

$\mathrm{d}I/\mathrm{d}V$ getting $D(\boldsymbol{r},V) = -\mathrm{d}^3I/\mathrm{d}V^3(\boldsymbol{r},V)$, which has been also applied to study the PDW in the cuprate.[134] In the two-dimensional case, the bidirectional property of the 3Q PDW on the hexagonal lattice is evidenced by the gap map and the corresponding Fourier transform (Fig. 16(e)), similar to the results in cuprates[131] and $NbSe_2$.[133]

To gain further understanding of the observed PDW, correlation between the modulation of zero-energy conductance $G_0(\boldsymbol{r})$ and coherence peak height $P(\boldsymbol{r})$ is studied. The modulations of $P(\boldsymbol{r})$ and $G_0(\boldsymbol{r})$ are out of phase, while the modulations of $P(\boldsymbol{r})$ and the gap-depth ($H(\boldsymbol{r}) = P(\boldsymbol{r}) - G_0(\boldsymbol{r})$) are in phase [Fig. 16(c)]. Because coherence peak height $P(\boldsymbol{r})$ has the positive correlation with the superfluid density[135] and $G_0(\boldsymbol{r})$ is associated with the normal fluid density, the relations between $P(\boldsymbol{r})$, $H(\boldsymbol{r})$ and $G_0(\boldsymbol{r})$ present an unprecedented electronic density wave modulation of superconductivity. Therefore, the as-observed PDW exhibits similar behaviors with the shallow roton minimum, where they are spatially modulated at the same vector $Q_{\mathrm{pdw}} = Q_{\mathrm{roton}} = Q_{3q-4a/3}$. The superfluid density and normal fluid density naturally emerge as anti-correlated on the vortex-antivortex lattice, accounting for the spatial modulation of zero-bias conductance and coherence peak height. The commensurate hexagonal vortex–antivortex lattice, which is from the zeros of the complex order parameter of PDW, forms the roton-PDW [Fig. 16(f)].

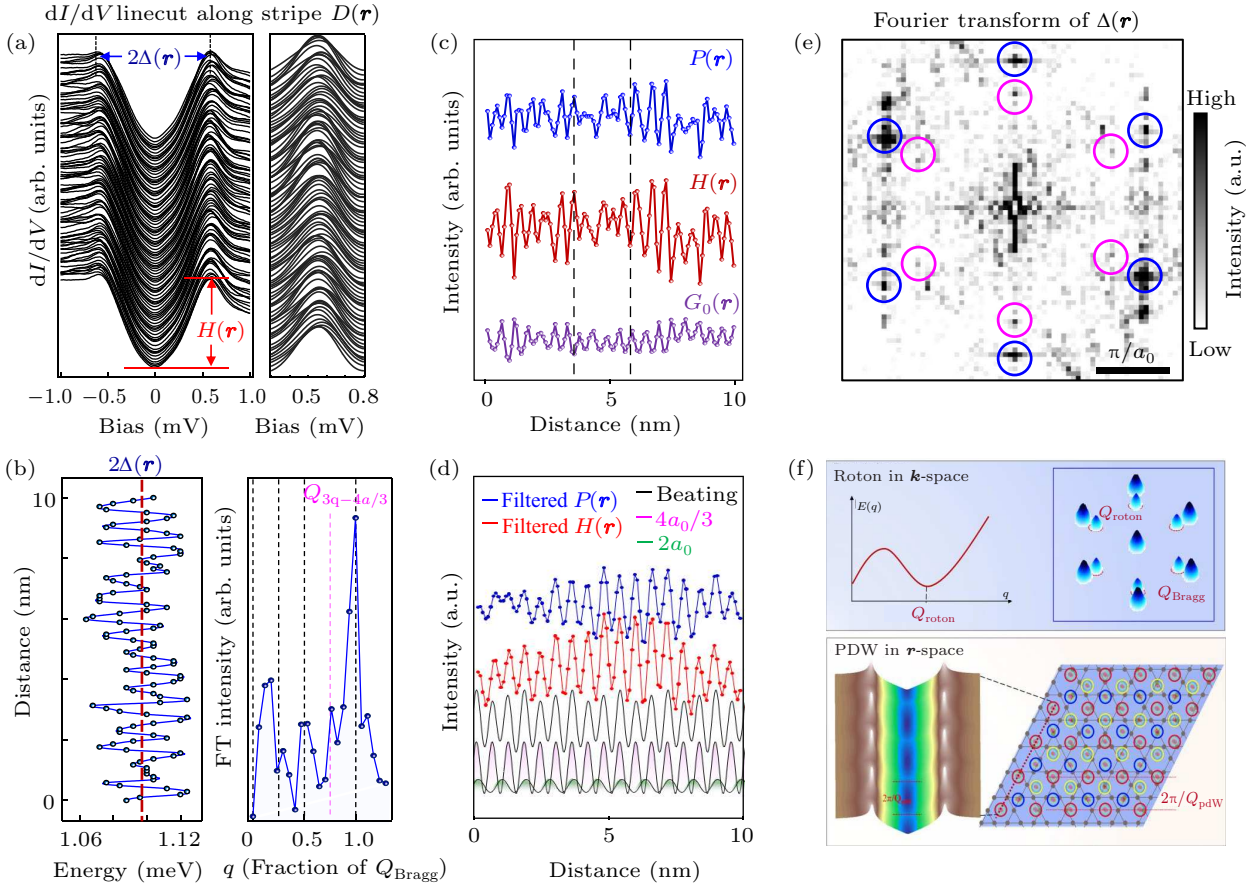


Fig. 16. Spectroscopic evidence of PDW at $Q_{3q-4a/3}$ in CsV_3Sb_5. (a) Evolution of the differential conductance $\mathrm{d}I/\mathrm{d}V(\boldsymbol{r},V)$ and negative of its second derivative $D(\boldsymbol{r},V) = -\mathrm{d}^3I/\mathrm{d}V^3(\boldsymbol{r},V)$ along a linecut in q_b-direction, respectively. (b) Plot of $2\Delta(\boldsymbol{r})$ and the corresponding Fourier spectrum, showing the $4a/3$ spatial modulation highlighted by the pink dashed line marked by $Q_{3q-4a/3}$. (c) Spatial modulations of coherence peak height $P(\boldsymbol{r})$, SC gap depth $H(\boldsymbol{r})$, and zero-bias conductance $G(\boldsymbol{r})$. The spectra are offset for clarity. (d) Beating pattern simulated using Q_{3q-2a} (green curve) and $Q_{3q-4a/3}$ (pink curve), showing consistency with Bragg-filtered modulations of $P(\boldsymbol{r})$ and $H(\boldsymbol{r})$. (e) Superconducting gap map $\Delta(\boldsymbol{r})$. (e) Fourier transform of superconducting gap map $\Delta(r)$, showing clearly $Q_{3q-4a/3}$ modulations of gap size. (f) Schematic illustration of the roton-PDW (adapted from Ref. [19]).

Generally, the PDW can exist in a system where the long-range CDWs and superconductivity coexist, since CDW can induce a PDW state in the context of Ginzburg–Landau theory as well.[133] However, the PDW in *A*VS can serves as a 'mother state' corresponding to the pseudogap analogizing to the theory of 'mother state' in cuprates as proposed by P. A. Lee[136] according to the following evidence: (1) There is a suppression of LDOS over ±5 meV in the spatially average spectrum at distinct magnetic field and temperature, which corresponds to a possible pseudogap phase [Fig. 17(a)]. (2) In contrast to the 1×4 and 2×2 CDW peaks that exist at all energies, the nondispersive $3Q$-$4a/3$ order is visible only in the energy range of pseudogap (∼ ±5 meV). (3) PDW survives in the magnetic-field-induced Abrikosov vortex halo region, contrasting to the one in the cuprate where the $8a$ PDW only manifests in the vortex halo when the superconductivity

is suppressed[137] [Fig. 17(b)]. (4) In the magnetic field above H_{c2} ($B_z = 2$ T) and at the electron temperature of 300 mK, all $3Q$ PDW, 2×2 CDW, and $4a$ stripe charge order persist and define a state of 'zero-temperature' pseudogap phase [Fig. 17(c)]. Based on the Ginzburg–Landau theory, the 3Q PDW living on a hexagonal lattice can produce a subsidiary CDW by the coupling of the order parameters of $3Q$ PDW with itself. Under the hexagonal symmetry, the CDW with $\psi_{2Q_p^\alpha}$ has the wave vector $2Q_p^\alpha = \frac{3}{2}Q_{\rm Bragg}^\alpha$ which is nothing but the 2×2 CDW manifest in the second Brillouin zone, while the CDW with $\psi_{Q_p^\alpha - Q_p^\beta}$ harbors the wave vector $Q_p^\alpha - Q_p^\beta = Q_p^\gamma$ which is coincident with the other modulation of the three PDW.

When warming the sample up to 4.2 K, the $\mathrm{d}I/\mathrm{d}V$ map remains all the charge order as observed in the superconducting state, implying that the PDW state can coexist with other intertwined charge orders in the normal state [Fig. 17(d)]. The peak around $\sim\pm5$ meV manifesting as the magnitude of the pseudogap becomes sharper when the system going into a superconducting state, especially in the condition of the 0 T magnetic field [Fig. 17(a)]). Despite that the PDW itself is not coherent, the order parameter of PDW can couple to the SC condensate Δ_{SC} to transform the incoherent peak into coherent when stepping into SC state. It is the best explanation to correspond such a peak to the PDW since a CDW should almost preserve its peak shape both in the normal state and the superconducting state. Besides, the pseudogap size itself also exhibits spatial modulations at the $3Q$ $Q_{3q-4a/3}$ wave vector [Fig. 17(e)], further demonstrating the $3Q$ PDW associated with the pseudogap as a mother state.

Recently, quantum oscillations with periodicities of $h/4e$ and $h/6e$ are discovered in CsV_3Sb_5, providing direct evidence for the existence of charge-4e and charge-6e superconducting condensate.[138] Charge-2e, charge-4e and charge-6e superconducting condensate exist in different temperature regions, below 1.0 K for charge-2e, $1.0\sim2.3$ K for charge-4e and 2.3 K $\sim T_c$ for charge-6e, respectively. The charge-4e and charge-6e superconducting are possible vestigial electronic ordered states. The charge-2e roton PDW state is revealed at ~0.3 K. It is proposed that deep in the PDW state, both translation and rotation symmetry are broken. As the temperature increases, the rotation symmetry and translation symmetry restore in sequence, leading to existence of charge-4e and charge-6e superconductivity, respectively.

The roton-PDW is discovered in CsV_3Sb_5, which satisfies the definition of PDW and behaves like a roton with anti-correlation to the superfluid density. Such a novel PDW is distinct from the trivial one which can be deduced from the CDW in the superconducting state, serving as a "mother state" corresponding to the pseudogap and can generate subsidiary CDW in charge sector which can be detected by STM in our case. This PDW also survives in the normal state and "zero-temperature" phase where the superconductivity is removed, manifesting itself as a density wave of the preformed Cooper pair, making the AV_3Sb_5 family a promising platform to further study the mechanism of pair density wave superconductivity.[139,140]

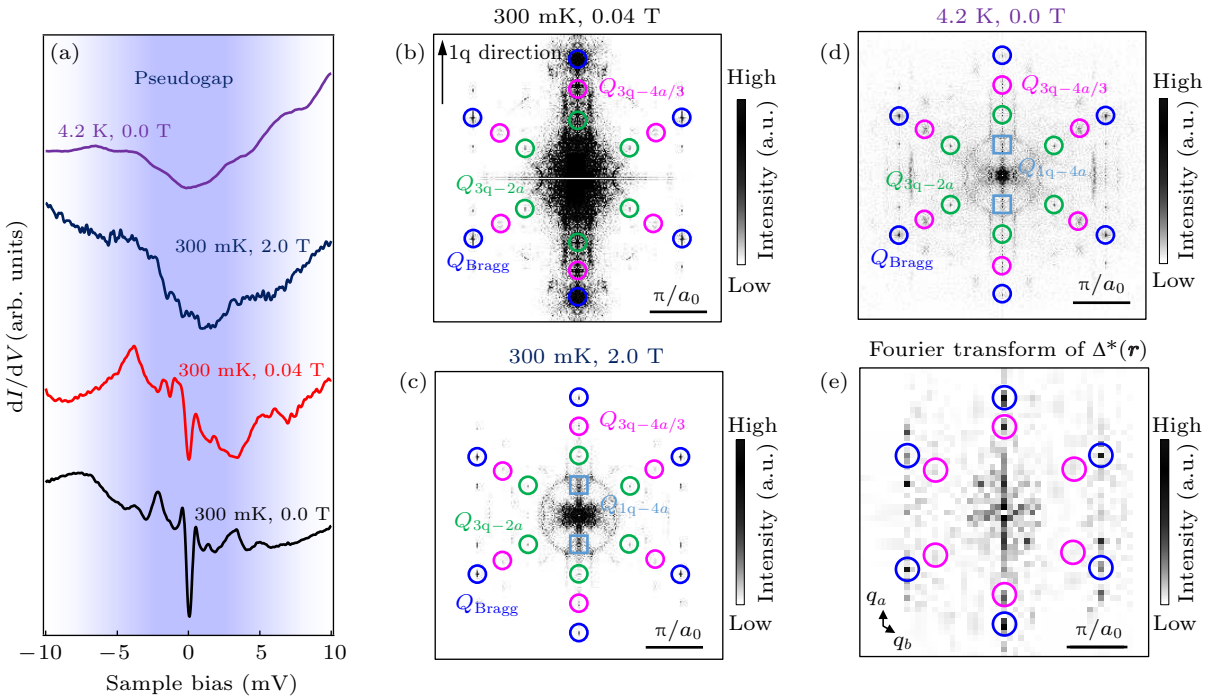


Fig. 17. Spectroscopic evidence of 'mother state' PDW corresponding to the pseudogap. (a) Spatially-averaged $\mathrm{d}I/\mathrm{d}V$ spectra obtained under different physical conditions of magnetic field and temperature, showing the spectral changes and the presence of the low energy pseudogap. (b)–(d) The magnitude of drift-corrected, two-fold symmetrized Fourier transform $\mathrm{d}I/\mathrm{d}V(\boldsymbol{r},-5\ \mathrm{mV})$ map at 300 mK, 0.04 T (b), 300 mK, 2.0 T (c) and 4.2 K, 0.0 T (d), respectively, showing the appearance of the density wave at $Q_{3q-4a/3}$ under distinct conditions. (e) Fourier transform of the pseudogap map showing peaks at the PDW vectors $Q_{3q-4a/3}$ circled in magenta (adapted from Ref. [19]).

7. Summary and outlook

In this review, we summarize the recent progress on the AV_3Sb_5 kagome materials. We focus on the main properties of AV_3Sb_5 in four aspects: (1) Giant AHE is demonstrated in AV_3Sb_5, showing the biggest Hall conductivity in kagome materials, but its origin is still unknown. (2) CDW shows unconventional behaviors, where the 2×2 CDW exhibiting time-reversal symmetry breaking may be associated with the giant AHE and the mechanism needs further exploration, the $4a$ stripe charge order (under the debate whether coming from bulk or surface) is nontrivial as well. (3) Unconventional strong coupling superconductivity encounter with Z_2 topology can provide possible Majorana zero mode despite the superconductor gap function is still unclear, and the competition between CDW and SC provides more details to uncover the hidden physics. (4) Intrinsic PDW brings non-trivial properties, such as a roton-like behavior manifesting the anti-correlation between superfluid density and normal fluid density, serving as a "mother state" corresponding to the pseudogap which can produce CDW in the same wave vector. The discovery of AV_3Sb_5 kagome materials not only enriches the research of exploring the next-generation quantum device but also appeals plenty of fundamental research interests, providing a fertile platform to study the interplay among AHE, topology, flat band, CDW, SC, and PDW. All the above physics phenomena emerge at distinct temperature ranges in CsV_3Sb_5, one representative material in AV_3Sb_5family, are plotted as a summary graph in Fig. 18.

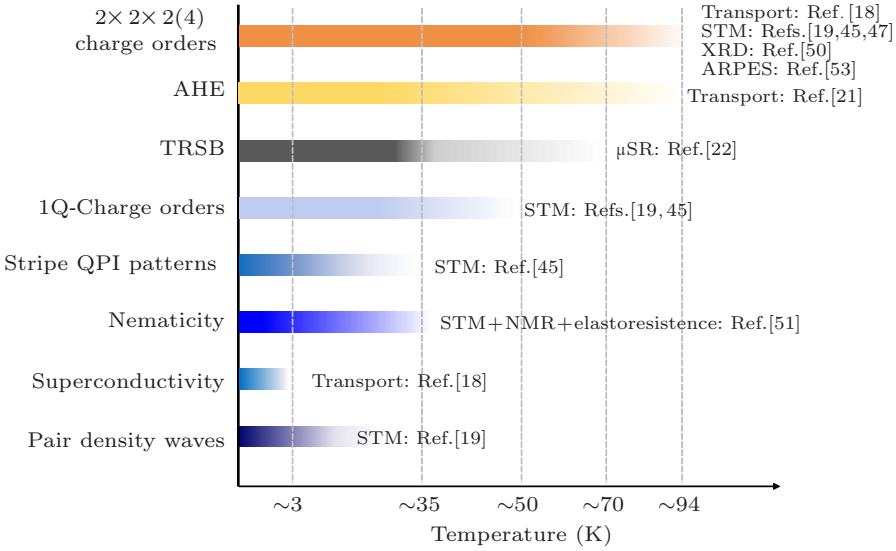


Fig. 18. Summary of the emergence of exotic physical phenomenon in CsV_3Sb_5 at distinct temperature ranges (the temperature ranges are taken from the references as labeled).

Despite many experimental results that have been included in the review, some works are still in progress and an abundance of unconventional properties are to be explored in this field.

First, the origin of CDW should be further determined, including both $2 \times 2 \times 2(4)$ and $4a$ CDW. The relations among time-reversal symmetry breaking, 2×2 CDW, and AHE are waiting to be uncovered both on the experimental side and theoretical side. Although some theoretics propose diverse models[26,46,67–69,77] to try to understand all the physics related to the CDWs, a complete solution to reconcile all experimental results and predicting new phenomena is still lacking. Besides, contradicting experimental results[39,70,78] on the determination of the chiral CDW should be explained in a consistent way. A similar debate[19,45,75] on the origin of the $4a$ stripe charge order is also calling for more works in the future. Very recently, CDW has been discovered within an antiferromagnetic ordered phase of kagome lattice FeGe by neutron scattering[141] and STM.[142] The CDWs are found to share many features with AV_3Sb_5 but show distinct features such as strong correlation driven band renormalizations, appearance of edge states and enhancement of the magnetic moments below the CDW transition temperature.[143] The newly discovered CDWs in FeGe indicate the universal origin of charge orders in both superconducting and magnetic kagome materials.

Second, the SC gap function and the band structure below SC T_c require more studies. So far, it is difficult to study the band structure at the superconducting state as most APRES instruments work at a temperature higher than $T_c \sim 2.5$ K. One of the solutions is to increase the SC transition temperature, such as applying pressure and reduce the sample thickness as introduced in Section 5. Moreover, the layered structure in AV_3Sb_5 with Van de Waals interlayer coupling provides further opportunities to obtain one-unit cell two-dimensional kagome materials by exfoliation for deeper exploration of these and other unexpected challenges in the low-energy many-body physics.

Third, more investigations related to PDW, such as the π phase winding in the PDW order near the CDW dislocation and the Josephson tunneling process related to the Cooper pair detection, should be put on the agenda. The real roton mode related to the bosonic excitation is elusive. Such a mode can be detected in the tunneling process through the electron-mode coupling, as many kinds of bosonic modes were verified by different STM groups[144–147] in the past. Furthermore, the band structure of PDW needs more investigations as well.

Finally, the discovery of AV_3Sb_5 inspires exploration of more quantum materials based on kagome lattices. New families of V-based kagome compounds such as ReV_6Sn_6 (Re = Gd, Ho),[148] V_3Sb_2,[149] V_6Sb_4,[150] AV_6Sb_6[151] and AV_8Sb_{12}[152,153] have recently been proposed and partially synthesized. In addition, a series of candidate kagome superconductors based on AV_3Sb_5 crystal structure are also predicted.[154,155] Except for the 135 system, new flat band materials hosting kagome sublattices[156] have been recently predicted.

In general, the study of kagome materials itself is a promising research field with plenty of exotic properties. When the kagome structure meets with multiple electronic orders, a plethora of new phenomena emerge and appeal a diversity of researchers joining from different research fields. We expect new discoveries for new physics and applications based on this family of materials.

Acknowledgments

We are grateful to Profs. Ziqiang Wang, Sen Zhou, Xiaoli Dong, Fang Zhou, Li Yu, Yan Zhang, Lin Zhao, Xinjiang Zhou, Rui Zhou, Qingming Zhang, Binghai Yan, Kun Jiang, Jiangping Hu for helpful discussions and suggestion. We acknowledge the financial support from the Ministry of Science and Technology of China, the National Natural Science Foundation of China and Chinese Academy of Sciences.

References

[1] Syôzi I 1951 *Prog. Theor. Phys.* **6** 306
[2] Balents L 2010 *Nature* **464** 199
[3] Helton J S, Matan K, Shores M P, Nytko E A, Bartlett B M, Yoshida Y, Takano Y, Suslov A, Qiu Y, Chung J H, Nocera D G and Lee Y S 2007 *Phys. Rev. Lett.* **98** 107204
[4] Ko W H, Lee P A and Wen X G 2009 *Phys. Rev. B* **79** 214502
[5] Han T H, Helton J S, Chu S, Nocera D G, Rodriguez-Rivera J A, Broholm C and Lee Y S 2012 *Nature* **492** 406
[6] Fu M, Imai T, Han T H and Lee Young S 2015 *Science* **350** 655
[7] Ye L, Kang M, Liu J, von Cube F, Wicker C R, Suzuki T, Jozwiak C, Bostwick A, Rotenberg E, Bell D C, Fu L, Comin R and Checkelsky J G 2018 *Nature* **555** 638
[8] Yin J X, Zhang S S, Li H, *et al.* 2018 *Nature* **562** 91
[9] Liu Z, Li M, Wang Q, Wang G, Wen C, Jiang K, Lu X, Yan S, Huang Y, Shen D, Yin J X, Wang Z, Yin Z, Lei H and Wang S 2020 *Nat. Commun.* **11** 4002
[10] Morali N, Batabyal R, Nag Pranab K, Liu E, Xu Q, Sun Y, Yan B, Felser C, Avraham N and Beidenkopf H 2019 *Science* **365** 1286
[11] Liu D F, Liang A J, Liu E K, Xu Q N, Li Y W, Chen C, Pei D, Shi W J, Mo S K, Dudin P, Kim T, Cacho C, Li G, Sun Y, Yang L X, Liu Z K, Parkin S S P, Felser C and Chen Y L 2019 *Science* **365** 1282
[12] Kuroda K, Tomita T, Suzuki M T, *et al.* 2017 *Nat. Mater.* **16** 1090
[13] Yin J X, Ma W, Cochran T A, *et al.* 2020 *Nature* **583** 533
[14] Yin J X, Zhang S S, Chang G, *et al.* 2019 *Nat. Phys.* **15** 443
[15] Nakatsuji S, Kiyohara N and Higo T 2015 *Nature* **527** 212
[16] Xing Y, Shen J, Chen H, *et al.* 2020 *Nat. Commun.* **11** 5613
[17] Ortiz B R, Gomes L C, Morey J R, Winiarski M, Bordelon M, Mangum J S, Oswald I W H, Rodriguez-Rivera J A, Neilson J R, Wilson S D, Ertekin E, McQueen T M and Toberer E S 2019 *Phys. Rev. Mater.* **3** 094407
[18] Ortiz B R, Teicher S M L, Hu Y, Zuo J L, Sarte P M, Schueller E C, Abeykoon A M M, Krogstad M J, Rosenkranz S, Osborn R, Seshadri R, Balents L, He J and Wilson S D 2020 *Phys. Rev. Lett.* **125** 247002
[19] Chen H, Yang H, Hu B, *et al.* 2021 *Nature* **599** 222
[20] Chen K Y, Wang N N, Yin Q W, Gu Y H, Jiang K, Tu Z J, Gong C S, Uwatoko Y, Sun J P, Lei H C, Hu J P and Cheng J G 2021 *Phys. Rev. Lett.* **126** 247001
[21] Yu F H, Wu T, Wang Z Y, Lei B, Zhuo W Z, Ying J J and Chen X H 2021 *Phys. Rev. B* **104** L041103
[22] Yu L, Wang C, Zhang Y, *et al.* 2021 arXiv: 2107.10714 [cond]
[23] Shumiya N, Hossain M S, Yin J X, *et al.* 2021 *Phys. Rev. B* **104** 035131
[24] Mielke C, Das D, Yin J X, *et al.* 2022 *Nature* **602** 245
[25] Xu H S, Yan Y J, Yin R, Xia W, Fang S, Chen Z, Li Y, Yang W, Guo Y and Feng D L 2021 *Phys. Rev. Lett.* **127** 187004
[26] Wu X, Schwemmer T, Müller T, Consiglio A, Sangiovanni G, Di Sante D, Iqbal Y, Hanke W, Schnyder A P, Denner M M, Fischer M H, Neupert T and Thomale R 2021 *Phys. Rev. Lett.* **127** 177001
[27] Song B Q, Kong X M, Xia W, Yin Q W, Tu C P, Zhao C C, Dai D Z, Meng K, Tao Z C, Tu Z J, Gong C S, Lei H C, Guo Y F, Yang X F and Li S Y 2021 arXiv: 2105.09248 [cond]
[28] Song Y, Ying T, Chen X, Han X, Wu X, Schnyder A P, Huang Y, Guo J G and Chen X 2021 *Phys. Rev. Lett.* **127** 237001
[29] Qian T, Christensen M H, Hu C, Saha A, Andersen B M, Fernandes R M, Birol T and Ni N 2021 *Phys. Rev. B* **104** 144506
[30] Nagaosa N, Sinova J, Onoda S, MacDonald A H and Ong N P 2010 *Rev. Mod. Phys.* **82** 1539
[31] Weng H, Yu R, Hu X, Dai X and Fang Z 2015 *Adv. Phys.* **64** 227
[32] Liu E, Sun Y, Kumar N, *et al.* 2018 *Nat. Phys.* **14** 1125
[33] Asaba T, Thomas S M, Curtis M, Thompson J D, Bauer E D and Ronning F 2020 *Phys. Rev. B* **101** 174415
[34] Manna K, Sun Y, Muechler L, Kübler J and Felser C 2018 *Nat. Rev. Mater.* **3** 244
[35] Sakai A, Mizuta Y P, Nugroho A A, Sihombing R, Koretsune T, Suzuki M T, Takemori N, Ishii R, Nishio-Hamane D, Arita R, Goswami P and Nakatsuji S 2018 *Nat. Phys.* **14** 1119
[36] Yang S Y, Wang Y, Ortiz B R, Liu D, Gayles J, Derunova E, Gonzalez-Hernandez R, Šmejkal L, Chen Y, Parkin S S P, Wilson S D, Toberer E S, McQueen T and Ali M N 2020 *Sci. Adv.* **6** eabb6003
[37] Wei Q, Yin Z T, Gong C S, Fu Y, Yan S H and Lei H 2021 *Chin. Phys. Lett.* **38** 037403
[38] Kenney E M, Ortiz B R, Wang C, Wilson S D and Graf M J 2021 *J. Condens. Matter Phys.* **33** 235801
[39] Jiang Y X, Yin J X, Denner M M, *et al.* 2021 *Nat. Mater.* **20** 1353
[40] Grüner G 2018 *Density waves in solids* (CRC Press)
[41] Calandra M, Mazin I and Mauri F 2009 *Phys. Rev. B* **80** 241108
[42] Rice T M and Scott G K 1975 *Phys. Rev. Lett.* **35** 120
[43] van Wezel J, Nahai-Williamson P and Saxena S S 2010 *Phys. Rev. B* **81** 165109
[44] Gerber S, Jang H, Nojiri H, Matsuzawa S, Yasumura H, Bonn D, Liang R, Hardy W, Islam Z and Mehta A 2015 *Science* **350** 949
[45] Zhao H, Li H, Ortiz B R, Teicher S M L, Park T, Ye M, Wang Z, Balents L, Wilson S D and Zeljkovic I 2021 *Nature* **599** 216
[46] Tan H, Liu Y, Wang Z and Yan B 2021 *Phys. Rev. Lett.* **127** 046401
[47] Liang Z, Hou X, Zhang F, Ma W, Wu P, Zhang Z, Yu F, Ying J J, Jiang K, Shan L, Wang Z and Chen X H 2021 *Phys. Rev. X* **11** 031026
[48] Ratcliff N, Hallett L, Ortiz B R, Wilson S D and Harter J W 2021 *Phys. Rev. Mater.* **5** L111801
[49] Luo J, Zhao Z, Zhou Y Z, Yang J, Fang A F, Yang H T, Gao H J, Zhou R and Zheng G Q 2022 *npj Quantum Mater.* **7** 30
[50] Li H, Zhang T T, Yilmaz T, Pai Y Y, Marvinney C E, Said A, Yin Q W, Gong C S, Tu Z J, Vescovo E, Nelson C S, Moore R G, Murakami S, Lei H C, Lee H N, Lawrie B J and Miao H 2021 *Phys. Rev. X* **11** 031050
[51] Nie L, Sun K, Ma W, *et al.* 2022 *Nature* **604** 59

[52] Ortiz B R, Teicher S M L, Kautzsch L, Sarte P M, Ratcliff N, Harter J, Ruff J P C, Seshadri R and Wilson S D 2021 *Phys. Rev. X* **11** 041030

[53] Kang M, Fang S, Yoo J, Ortiz B R, Oey Y, Ryu S H, Kim J, Jozwiak C, Bostwick A, Rotenberg E, Kaxiras E, Checkelsky J, Wilson S D, Park J H and Comin R 2022 arXiv: 2202.01902

[54] Kang M, Fang S, Kim J K, Ortiz B R, Ryu S H, Kim J, Yoo J, Sangiovanni G, Di Sante D, Park B G, Jozwiak C, Bostwick A, Rotenberg E, Kaxiras E, Wilson S D, Park J H and Comin R 2022 *Nat. Phys.* **18** 301

[55] Hu Y, Wu X, Ortiz B R, Ju S, Han X, Ma J Z, Plumb N C, Radovic M, Thomale R, Wilson S D, Schnyder A P and Shi M 2021 arXiv: 2106.05922 [cond]

[56] Cho S, Ma H, Xia W, Yang Y, Liu Z, Huang Z, Jiang Z, Lu X, Liu J, Liu Z, Li J, Wang J, Liu Y, Jia J, Guo Y, Liu J and Shen D 2021 *Phys. Rev. Lett.* **127** 236401

[57] Wang Z, Ma S, Zhang Y, Yang H, Zhao Z, Ou Y, Zhu Y, Ni S, Lu Z, Chen H, Jiang K, Yu L, Zhang Y, Dong X, Hu J, Gao H J and Zhao Z 2021 arXiv: 2104.05556 [cond]

[58] Luo H, Gao Q, Liu H, *et al.* 2022 *Nat. Commun.* **13** 273

[59] Uykur E, Ortiz B R, Wilson S D, Dressel M and Tsirlin A A 2022 *npj Quantum Mater.* **7** 16

[60] Xie Y, Li Y, Bourges P, Ivanov A, Ye Z, Yin J X, Hasan M Z, Luo A, Yao Y, Wang Z, Xu G and Dai P 2022 *Phys. Rev. B* **105** L140501

[61] Liu G, Ma X, He K, Li Q, Tan H, Liu Y, Xu J, Tang W, Watannabe K, Taniguchi T, Gao L, Dai Y, Wen H H, Yan B and Xi X 2022 arXiv: 2201.05330

[62] Wang Z X, Wu Q, Yin Q W, Gong C S, Tu Z J, Lin T, Liu Q M, Shi L Y, Zhang S J, Wu D, Lei H C, Dong T and Wang N L 2021 *Phys. Rev. B* **104** 165110

[63] Song D, Zheng L, Yu F, Li J, Nie L, Shan M, Zhao D, Li S, Kang B, Wu Z, Zhou Y, Sun K, Liu K, Luo X, Wang Z, Ying J, Wan X, Wu T and Chen X 2022 *Sci. China: Phys. Mech. Astron.* **65** 247462

[64] Liu Z, Zhao N, Yin Q, Gong C, Tu Z, Li M, Song W, Liu Z, Shen D, Huang Y, Liu K, Lei H and Wang S 2021 *Phys. Rev. X* **11** 041010

[65] Nakayama K, Li Y, Kato T, Liu M, Wang Z, Takahashi T, Yao Y and Sato T 2021 *Phys. Rev. B* **104** L161112

[66] Hu Y, Wu X, Ortiz B R, Han X, Plumb N C, Wilson S D, Schnyder A P and Shi M 2022 Arxiv: 2201.06477

[67] Feng X, Jiang K, Wang Z and Hu J 2021 *Sci. Bull.* **66** 1384

[68] Denner M M, Thomale R and Neupert T 2021 *Phys. Rev. Lett.* **127** 217601

[69] Park T, Ye M and Balents L 2021 *Phys. Rev. B* **104** 035142

[70] Li H, Zhao H, Ortiz B R, Park T, Ye M, Balents L, Wang Z, Wilson S D and Zeljkovic I 2022 *Nat. Phys.* **18** 265

[71] Li H, Zhao H, Ortiz B, Oey Y, Wang Z, Wilson S D and Zeljkovic I 2022 arXiv: 2203.15057 [cond]

[72] Bin Hu Y Y, Huang Z H, Han X H, Zhao Z, Yang H T, Chen H and Gao H J 2022 *Chin. Phys. B* **31** 58102

[73] Zhang D, Ha J, Baek H, Chan Y H, Natterer F D, Myers A F, Schumacher J D, Cullen W G, Davydov A V, Kuk Y, Chou M Y, Zhitenev N B and Stroscio J A 2017 *Phys. Rev. Mater.* **1** 024005

[74] Gao S, Flicker F, Sankar R, Zhao H, Ren Z, Rachmilowitz B, Balachandar S, Chou F, Burch K S, Wang Z, van Wezel J and Zeljkovic I 2018 *Proc. Natl. Acad. Sci. USA* **115** 6986

[75] Wang Z, Jiang Y X, Yin J X, *et al.* 2021 *Phys. Rev. B* **104** 075148

[76] Xiang Y, Li Q, Li Y, Xie W, Yang H, Wang Z, Yao Y and Wen H H 2021 *Nat. Commun.* **12** 6727

[77] Feng X, Zhang Y, Jiang K and Hu J 2021 *Phys. Rev. B* **104** 165136

[78] Li H, Wan S, Li H, Li Q, Gu Q, Yang H, Li Y, Wang Z, Yao Y and Wen H H 2022 *Phys. Rev. B* **105** 045102

[79] Xu Y, Ni Z, Liu Y, Ortiz B R, Wilson S D, Yan B, Balents L and Wu L 2022 arXiv e-prints arXiv: 2204.10116

[80] Wu Q, Wang Z X, Liu Q M, Li R S, Xu S X, Yin Q W, Gong C S, Tu Z J, Lei H C, Dong T and Wang N L 2021 arXiv e-prints arXiv: 2110.11306

[81] Zhou X, Li Y, Fan X, Hao J, Dai Y, Wang Z, Yao Y and Wen H H 2021 *Phys. Rev. B* **104** L041101

[82] Lin Y P and Nandkishore R M 2021 *Phys. Rev. B* **104** 045122

[83] Bardeen J, Cooper L N and Schrieffer J R 1957 *Phys. Rev.* **108** 1175

[84] Ginzburg V L 2009 *On Superconductivity and Superfluidity* (New York: Springer)

[85] Tinkham M 2004 *Introduction to Superconductivity*, 2nd edn. (New York: Mineola) pp. 127–130

[86] Balents L, Dean C R, Efetov D K and Young A F 2020 *Nat. Phys.* **16** 725

[87] Cao Y, Fatemi V, Fang S, Watanabe K, Taniguchi T, Kaxiras E and Jarillo-Herrero P 2018 *Nature* **556** 43

[88] Matthias B T, Geballe T H and Compton V B 1963 *Rev. Mod. Phys.* **35** 1

[89] Tsuei C C and Kirtley J R 2000 *Rev. Mod. Phys.* **72** 969

[90] Norman M R and Pépin C 2003 *Rep. Prog. Phys.* **66** 1547

[91] Taillefer L 2010 *Annu. Rev. Condens. Matter Phys.* **1** 51

[92] Ren Z A and Zhao Z X 2009 *Adv. Mater.* **21** 4584

[93] Zhang P, Wang Z, Wu X, Yaji K, Ishida Y, Kohama Y, Dai G, Sun Y, Bareille C and Kuroda K 2019 *Nat. Phys.* **15** 41

[94] Wang F and Lee D H 2011 *Science* **332** 200

[95] Winterlik J, Fecher G H, Felser C, Jourdan M, Grube K, Hardy F, von Löhneysen H, Holman K L and Cava R J 2008 *Phys. Rev. B* **78** 184506

[96] Ronning F, Bauer E D, Park T, Kurita N, Klimczuk T, Movshovich R, Sefat A S, Mandrus D and Thompson J D 2009 *Physica C* **469** 396

[97] Le C, Zeng J, Gu Y, Cao G H and Hu J 2018 *Sci. Bull.* **63** 957

[98] Wang D, Kong L, Fan P, Chen H, Zhu S, Liu W, Cao L, Sun Y, Du S, Schneeloch J, Zhong R, Gu G, Fu L, Ding H and Gao H J 2018 *Science* **362** 333

[99] Zhu S, Kong L, Cao L, Chen H, Papaj M, Du S, Xing Y, Liu W, Wang D, Shen C, Yang F, Schneeloch J, Zhong R, Gu G, Fu L, Zhang Y Y, Ding H and Gao H J 2020 *Science* **367** 189

[100] Liu W, Cao L, Zhu S, Kong L, Wang G, Papaj M, Zhang P, Liu Y B, Chen H and Li G 2020 *Nat. Commun.* **11** 1

[101] Kong L, Zhu S, Papaj M, Chen H, Cao L, Isobe H, Xing Y, Liu W, Wang D, Fan P, Sun Y, Du S, Schneeloch J, Zhong R, Gu G, Fu L, Gao H J and Ding H 2019 *Nat. Phys.* **15** 1181

[102] Hirvensalo M 2001 *Quantum Computing* (Berlin: Springer)

[103] Steane A 1998 *Rep. Prog. Phys.* **61** 117

[104] Ortiz B R, Sarte P M, Kenney E M, Graf M J, Teicher S M L, Seshadri R and Wilson S D 2021 *Phys. Rev. Mater.* **5** 034801

[105] Ni S, Ma S, Zhang Y, *et al.* 2021 *Chin. Phys. Lett.* **38** 057403

[106] Gupta R, Das D, III C H M, Guguchia Z, Shiroka T, Baines C, Bartkowiak M, Luetkens H, Khasanov R, Yin Q, Tu Z, Gong C and Lei H 2021 arXiv: 2108.01574

[107] Mu C, Yin Q, Tu Z, Gong C, Lei H, Li Z and Luo J 2021 *Chin. Phys. Lett.* **38** 077402

[108] Gu Y, Zhang Y, Feng X, Jiang K and Hu J 2022 *Phys. Rev. B* **105** L100502

[109] Hess H F, Robinson R B and Waszczak J V 1990 *Phys. Rev. Lett.* **64** 2711

[110] Xu J P, Wang M X, Liu Z L, Ge J F, Yang X, Liu C, Xu Z A, Guan D, Gao C L, Qian D, Liu Y, Wang Q H, Zhang F C, Xue Q K and Jia J F 2015 *Phys. Rev. Lett.* **114** 017001

[111] Hess H F, Robinson R B, Dynes R C, Valles J M and Waszczak J V 1989 *Phys. Rev. Lett.* **62** 214

[112] Yuan Y, Pan J, Wang X, Fang Y, Song C, Wang L, He K, Ma X, Zhang H, Huang F, Li W and Xue Q K 2019 *Nat. Phys.* **15** 1046

[113] Yu J, Xu Z, Xiao K, Yuan Y, Yin Q, Hu Z, Gong C, Guo Y, Tu Z, Tang P, Lei H, Xue Q K and Li W 2022 *Nano Lett.* **22** 918

[114] Hu Y, Teicher S M L, Ortiz B R, Luo Y, Peng S, Huai L, Ma J, Plumb N C, Wilson S D, He J and Shi M 2022 *Sci. Bull.* **67** 495

[115] Sentef M A, Tokuno A, Georges A and Kollath C 2017 *Phys. Rev. Lett.* **118** 087002

[116] Jaefari A, Lal S and Fradkin E 2010 *Phys. Rev. B* **82** 144531

[117] Singh Y, Nirmala R, Ramakrishnan S and Malik S 2005 *Phys. Rev. B* **72** 045106

[118] Yu F H, Ma D H, Zhuo W Z, Liu S Q, Wen X K, Lei B, Ying J J and Chen X H 2021 *Nat. Commun.* **12** 3645

[119] Zhang Z, Chen Z, Zhou Y, Yuan Y, Wang S, Zhang L, Zhu X, Zhou Y, Chen X, Zhou J and Yang Z 2021 arXiv: 2103.12507 [cond]

[120] Wang N N, Chen K Y, Yin Q W, Ma Y N N, Pan B Y, Yang X, Ji X Y, Wu S L, Shan P F, Xu S X, Tu Z J, Gong C S, Liu G T, Li G, Uwatoko Y, Dong X L, Lei H C, Sun J P and Cheng J G 2021 arXiv: 2107.00269 [cond]

[121] Du F, Luo S, Ortiz B R, Chen Y, Duan W, Zhang D, Lu X, Wilson S D, Song Y and Yuan H 2021 *Phys. Rev. B* **103** L220504

[122] Zhu C C, Yang X F, Xia W, Yin Q W, Wang L S, Zhao C C, Dai D Z, Tu C P, Song B Q, Tao Z C, Tu Z J, Gong C S, Lei H C, Guo Y F and Li S Y 2021 *Phys. Rev. B* **105** 094507

[123] Yu F, Zhu X, Wen X, Gui Z, Li Z, Han Y, Wu T, Wang Z, Xiang Z, Qiao Z, Ying J and Chen X 2022 *Phys. Rev. Lett.* **128** 077001

[124] Guguchia Z, Mielke Iii C, Das D, *et al.* 2022 arXiv: 2202.07713 [cond]

[125] Wang Y, Yang S, Sivakumar P K, Ortiz B R, Teicher S M, Wu H, Srivastava A K, Garg C, Liu D and Parkin S S 2020 arXiv: 2012.05898 [cond]

[126] Oey Y M, Ortiz B R, Kaboudvand F, Frassineti J, Garcia E, Cong R, Sanna S, Mitrović V F, Seshadri R and Wilson S D 2022 *Phys. Rev. Mater.* **6** L041801

[127] Yang H, Zhang Y, Huang Z, Zhao Z, Shi J, Qian G, Hu B, Lu Z, Zhang H, Shen C, Lin X, Wang Z, Pennycook S J, Chen H, Dong X, Zhou W and Gao H J 2021 arXiv: 2110.11228 [cond]

[128] Li Y, Li Q, Fan X, Liu J, Feng Q, Liu M, Wang C, Yin J X, Duan J, Li X, Wang Z, Wen H H and Yao Y 2022 arXiv: 2203.03524 [cond]

[129] Yin L, Zhang D, Chen C, Ye G, Yu F, Ortiz B R, Luo S, Duan W, Su H, Ying J, Wilson S D, Chen X, Yuan H, Song Y and Lu X 2021 *Phys. Rev. B* **104** 174507

[130] Agterberg D F, Davis J C S, Edkins S D, Fradkin E, Van Harlingen D J, Kivelson S A, Lee P A, Radzihovsky L, Tranquada J M and Wang Y 2020 *Annu. Rev. Condens. Matter Phys.* **11** 231

[131] Du Z, Li H, Joo S H, Donoway E P, Lee J, Davis J C S, Gu G, Johnson P D and Fujita K 2020 *Nature* **580** 65

[132] Hamidian M H, Edkins S D, Joo S H, Kostin A, Eisaki H, Uchida S, Lawler M J, Kim E A, Mackenzie A P, Fujita K, Lee J and Davis J C 2016 *Nature* **532** 343

[133] Liu X, Chong Y X, Sharma R and Davis J C S 2021 *Science* **372** 1447

[134] Ruan W, Li X, Hu C, Hao Z, Li H, Cai P, Zhou X, Lee D H and Wang Y 2018 *Nat. Phys.* **14** 1178

[135] Cho D, Bastiaans K M, Chatzopoulos D, Gu G D and Allan M P 2019 *Nature* **571** 541

[136] Lee P A 2014 *Phys. Rev. X* **4** 031017

[137] Edkins S D, Kostin A, Fujita K, Mackenzie A P, Eisaki H, Uchida S, Sachdev S, Lawler M J, Kim E A, Davis J C S and Hamidian M H 2019 *Science* **364** 976

[138] Ge J, Wang P, Xing Y, Yin Q, Lei H, Wang Z and Wang J 2022 arXiv: 2201.10352 [cond]

[139] Zhou S and Wang Z 2021 arXiv: 2110.06266 [cond]

[140] Jin J T, Jiang K, Yao H and Zhou Y 2022 arXiv: 2204.05029 [cond]

[141] Teng X, Chen L, Ye F, *et al.* 2022 arXiv: 2203.11467 [cond]

[142] Yin J X, Jiang Y X, Teng X, *et al.* 2022 arXiv: 2203.01888 [cond]

[143] Setty C, Lane C A, Chen L, Hu H, Zhu J X and Si Q 2022 arXiv: 2203.01930 [cond]

[144] Niestemski F C, Kunwar S, Zhou S, Li S, Ding H, Wang Z, Dai P and Madhavan V 2007 *Nature* **450** 1058

[145] Wang Z, Huang C Y, Hsu C H, Namiki H, Chang T R, Chuang F C, Lin H, Sasagawa T, Madhavan V and Okada Y 2022 *Phys. Rev. B* **105** 075110

[146] Song C L, Wang Y L, Jiang Y P, Li Z, Wang L, He K, Chen X, Hoffman J E, Ma X C and Xue Q K 2014 *Phys. Rev. Lett.* **112** 057002

[147] Yin J X, Shumiya N, Mardanya S, *et al.* 2020 *Nat. Commun.* **11** 4003

[148] Peng S, Han Y, Pokharel G, Shen J, Li Z, Hashimoto M, Lu D, Ortiz B R, Luo Y, Li H, Guo M, Wang B, Cui S, Sun Z, Qiao Z, Wilson S D and He J 2021 *Phys. Rev. Lett.* **127** 266401

[149] Wang N N, Gu Y H, McGuire M A, Yan J Q, Shi L F, Cui Q, Chen K Y, Wang Y X, Zhang H, Yang H X, Dong X L, Jiang K, Hu J P, Wang B S, Sun J P and Cheng J G 2021 *Chin. Phys. B* **31** 017106

[150] Yang Y, Wang R, Shi M Z, Wang Z, Xiang Z and Chen X H 2022 *Phys. Rev. B* **105** 155102

[151] Yang Y, Wang R, Shi M Z, Wang Z, Xiang Z and Chen X H 2021 *Phys. Rev. B* **104** 245128

[152] Yu xin, Yang W F, Zhang Q H, Chen Z X, Chen X, Ying T P, Wu X X, Yang X F, Meng F Q, Li G, Li S Y, Gu L, Qian T, Andreas P. Schnyder, Guo J G and Chen X 2021 *Chin. Phys. Lett.* **38** 127102

[153] Wei Q, Yin Z T, Gong C S, Tian S J and Lei H 2021 *Chin. Phys. Lett.* **38** 127401

[154] Yu T, Jiang Z Y, Wang Y X, Lu T L, Meng S, Jiang K and Liu M 2022 *Chin. Phys. Lett.* **39** 047402

[155] Yi X W, Ma X Y, Zhang Z, Liao Z W, You J Y and Su G 2022 arXiv: 2202.05588 [cond]

[156] Regnault N, Xu Y, Li M R, Ma D S, Jovanovic M, Yazdani A, Parkin S S P, Felser C, Schoop L M, Ong N P, Cava R J, Elcoro L, Song Z D and Bernevig B A 2022 *Nature* **603** 824